

A Study of Silica-Surface Particle Interactions

Vernon A. Booth
B.S. Chemistry, California State University, Northridge, 1986

A thesis submitted to the faculty of the
Oregon Graduate Institute of Science & Technology
in partial fulfillment of the requirements for the degree

Master of Science
in
Chemistry

July 1994

The thesis "A Study of Silica-Surface Particle Interactions" by Vernon A. Booth has been examined and approved by the following Examination Committee:

✓ David W. Grainger /
Associate Professor
Thesis Advisor

Anthony E. Bell
Associate Professor

Shankar B. Rananavare
Assistant Professor

○ John C. Westall
Professor
Oregon State University

ABSTRACT

A Study of Silica-Surface Particle Interactions

Vernon A. Booth, M.S.

Thesis Advisor: David W. Grainger

In the manufacture of integrated circuits, a silica slurry is employed to polish silica wafer surfaces flat. Water is used to rinse the slurry from the wafer surface, which is then dried. Any residual particles remaining on the wafer surfaces after drying are especially difficult to remove.

This study seeks to utilize surface (colloid) chemical principles and techniques in order to improve the post-polish rinse and also to remove dried-on silica particles. The objectives of the study are:

- 1) to reduce the amount of residual slurry remaining after post-polish rinsing, and
- 2) to develop means to remove any post-rinsing residual slurry.

The first objective is classified as Rinsing Enhancement, the second can be classified as either Adhesion Reduction or Particle Removal.

Rinsing enhancement investigations attempt to correlate rinsing solution modifications (such as surfactant additives) to a reduction in the number of residual post-rinse particles. Poly(ethyleneoxide) (PEO) was shown to be the most effective of the twelve monomeric and polymeric additives tested.

Adhesion reduction investigations compare qualitative adhesive strengths of residual particles on surfaces as a function of rinsing solution conditions, which include the effects of surfactant additives. Many of the additives tested showed reduced adhesive strengths, but most of these also promoted undesirable aggregation of the slurry. PEO is the notable exception, reducing adhesive strengths provided that the polymers molecular weight is sufficiently high.

Particle removal investigations explore the dissolution of residual particles, as well as attempt to exploit fluid surface tension in order to extract adherent residual silica particles from surfaces. Dissolution by either hydrofluoric acid or potassium hydroxide solutions was successful. Extraction by surface tension was not successful at removing residual particles.

In addition to these three categories, direct quantitative measurements of inter-surface forces were made using Atomic Force Microscopy (AFM). These measurements investigated the effects of solution conditions and steric forces resulting from adsorption of poly(ethyleneoxide).

ACKNOWLEDGMENTS

I would like to acknowledge the help provided by and extend my gratitude to the following people:

Dr. Pavel Smejtek and Shanru Wang of Portland State University for zeta-potential measurements.

Yihan Liu and Dr. D. Fennell Evans (Department of Chemical Engineering & Material Science, and National Science Foundation Center for Interfacial Engineering, University of Minnesota) for generously providing their help, time, equipment, and facilities to make the AFM force/distance measurements.

Scott Lantz and Dr. Wayne Ford of Intel Surface Analysis Laboratories for XPS analysis of residual PEO.

Lou Hodes of Intel Fab 4 for preparation and provision of oxidized test wafers.

Will Hough of Intel Surface Analysis Laboratories for AFM analysis of surface roughness and particle size for the dissolution studies.

The Intel Research Council for funding this research, and to the following Intel associates for their insight, suggestions, and scrutiny: Dr. Eb Andideh, Dr. Casey Bennett, Dr. Don Danielson, Dr. Wayne Ford, Will Hough, Dr. Mike Oliver, and Dr. Leo Yau.

Dr. Eb Andideh (Project Mentor) of Intel Portland Technology Division for his help, insight and opportunities provided throughout this study.

Rosemary Burris, Kristine Roley, Maureen Sloan, Kathy Stewart, Mary Vatne, and Julianne Williams of the OGI library staff for their extraordinarily proficient, reliable and pleasant assistance.

Nancy Christie for the many favors, advice, and sanity checks.

Andrew Stein and Kevin Maloney for their valuable review, comments, and discussions regarding this manuscript and related oral presentations.

Drs. David W. Grainger, Anthony E. Bell, Shankar Rananavare, and John C. Westall for serving on my Thesis Committee.

Dr. David W. Grainger (Thesis Advisor) for his guidance, free reign, and for offering me this opportunity, and Dr. Val Anderson for laying the groundwork.

Tricia Bergman for pointing me in this direction. Patty Hawley for her motivating words of encouragement. (Figuratively, I presume, but I wasn't about to call her on it: "[if you don't] I will personally kick your butt so hard..."). Anne Averhoff for her forethought in preparing a much appreciated cache. And to my parents La Verne and Jimmie Booth for their continued support and encouragement.

TABLE OF CONTENTS

ABSTRACT	iii
ACKNOWLEDGMENTS	v
TABLE OF CONTENTS	vii
LIST OF TABLES	x
LIST OF FIGURES	xi
CHAPTER 1 INTRODUCTION	1
Background	1
Objectives and Overview	2
Summary of Results	3
CHAPTER 2 RELEVANT PRINCIPLES	4
Surface Chemistry	4
Silica Chemistry	11
Particle Bonding Mechanisms	12
van der Waals	12
Hydrogen Bonding	12
Capillary Adhesion	12
Hydrophobic Interaction	12
Cationic Bridging	12
Silanol Condensation	12
Liquid-Based Silica Particle Deposition Mechanisms - Entrainment	14

CHAPTER 3	EXPERIMENTAL MATERIALS AND METHODS	16
Water		16
Test Wafers		17
Hydroxylated (Hydrophilic) Test Wafers		17
Methylated (Hydrophobic) Test Wafers		17
SS-25 Slurry Characterization		19
SS-25 Slurry Zeta-Potential Measurements		21
TS-530 Methylated Silica Slurry		21
Contact Angle Measurements		21
Suspension Stability Determination		22
Slurry and Wafer Treatments		22
Separate-Treatment		22
Combined-Treatment		22
Silica Particle Deposition		22
Spin Coating		23
Dip Coating		23
Rinsing Enhancement		23
Particle Counting Techniques		23
Tencor Surfscan		23
Optical Microscopy		24
Qualitative Nature of "Statistics"		24
Atomic Force Microscopy Imaging		25
Adhesion Force Measurements		25
Sonication		25
Atomic Force Microscopy (AFM)		26
CHAPTER 4	EXPERIMENTAL INVESTIGATIONS	27
4.1	Dissolution of Adhered Particles	28
Dissolution in HF		29
Dissolution in KOH		30

4.2	Extraction of Particles by Passage Through A Fluid Interface	32
	Mechanism and Rationale	32
4.3	Displacement of Wet Particles by Isopropanol	38
4.4	Adhesion Prevention via Chemical or Physical Bonding Inhibitors	40
	Silanized Surfaces and Controlled Bonding Experiments	41
	Alternative Caustic Media	45
	ethanolamine	45
	cholinehydroxide	45
	tetramethylammonium hydroxide (TMAH)	45
	Surfactant Adsorption	47
	Hydrogen-Bond Inhibiting Solutes	47
	Guanidine HCL	47
	Glycerol	47
	Micro Lab Soap®	47
	Cationic Surfactant CTAB	49
	Polymer Surface-Active Agents	51
	Nonionic Polymer PVA	53
	Synergistic Nonionic Polymer & Cationic Monomer, PVA & CTAB	53
	Amphoteric Polymer PEI	55
	Nonionic Polymer PEO	57
	Nonionic Block Copolymer PEO-PPO-PEO	63
	CHAPTER 5 AFM MEASUREMENT OF ADHESIVE/REPULSIVE FORCES	64
	Influence of pH and Ionic Strength	66
	Influence of Adsorbed PEO	70
	CONCLUSION	75
	REFERENCES	76

LIST OF TABLES

Table 1. Adhesive strengths of particle bonding mechanisms.	13
Table 2. Physical and Chemical Quantities	20
Table 3. Zeta-potential of 1/100 SS-25 in phosphate/citrate/borate buffer.	21
Table 4. Extraction of Particles by Passage Through A Fluid Interface	37
Table 5. IPA Displacement of Wet Slurry, Data Summary	39
Table 6. Controlled Bonding Experiments Using Silanized Surfaces	43
Table 7. Alternative Caustic Media, Slurry-Particle Count/Area.	46
Table 8. Hydrogen Bonding Agents, Slurry-Particle Count/Area.	48
Table 9. Monomer Surface-Active Agents, Slurry-Particle Count/Area.	50
Table 10. General Information About Polymers Tested.	52
Table 11. PVA with CTAB Anchor, Slurry-Particle Count/Area.	54
Table 12. PEI Polymer Surface-Active Agents, Slurry-Particle Count/Area	56
Table 13. PEO Polymer Surface-Active Agents, Slurry-Particle Count/Area	60
Table 14. PEO and pH, Slurry-Particle Count/Area	61
Table 15. PEO-PPO-PEO, Slurry-Particle Count/Area	63

LIST OF FIGURES

Figure 1. Contact angles and surface tensions: A) Water droplet on a hydrophilic surface, B) Water droplet on a hydrophobic surface, C) Stationary hydrophilic.	5
Figure 2. Net energy of interaction arising from the combination of Born repulsion and van der Waals attraction	6
Figure 3. Zeta-potential and its relation to the double layer surrounding a negatively charged particle surface	8
Figure 4. DLVO prediction of net interaction energy verses separation distance arising from the combination of van der Waals attraction and double-layer	9
Figure 5. Various states of hydration and hydroxyl association. Silica being amorphous, the bulk "-O-" segments represent several -O-Si-O- segments	11
Figure 6. Entrainment of negatively charged particles.	15
Figure 7. Contact angle of silanized wafer surfaces. Hydrophilic silica wafers were immersed in dilute dichlorodimethylsilane in hexadecane	18
Figure 8. Particle size distribution of dried slurry. Particle size is determined from AFM images of dried particles deposited from 1/100 SS-25.	19
Figure 9. "Variation in solubility of silica with radius of curvature of surface. The positive radii of curvature are shown in cross section as particles	28
Figure 10. HF Wafer-oxide etch rate & 95% confidence interval	31
Figure 11. KOH Wafer-oxide etch rate & 95% confidence interval	31

Figure 12. HF. Left abscissa: particle count/area, average particle size and standard deviation. Right abscissa: wafer roughness.	31
Figure 13. KOH. Left abscissa: particle count/area, average particle size and standard deviation. Right abscissa: wafer roughness.	31
Figure 14. Components of the restoration force	33
Figure 15. Components of extraction or compression forces	35
Figure 16. Displacement of wet particles by IPA. Entrainment of particles is inhibited. The IPA condensate displaces the particle laden water as the wafer	39
Figure 17. Entrainment of negatively charged particles. Suspended particles deposit onto a negatively charged hydrophilic wafer as the wetting water film	39
Figure 18. PEO molecular weight dependence for rinsing and adhesion strength in combined-treatment trials. PEO consistently shows enhancement	57
Figure 19. XPS data for various cleaning techniques. The black bars indicate XPS signal (287.0 eV) strength of the PEO C-O bonds.	62
Figure 20. Schematic and explanation of AFM measurement apparatus.	65
Figure 21. AFM Force-Distance Profiles: approaching surfaces, Si ₃ N ₄ tip #1 and #2 data, and HF etched SiO ₂ wafer	68
Figure 22. AFM Force-Distance Profiles: retracting surfaces, Si ₃ N ₄ tip #1 and #2 data, and HF etched SiO ₂ wafer. Note scale change	69
Figure 23. Electrostatic repulsive force decreases with increasing electrolyte concentration, as expected	71
Figure 24. Retraction traces are very similar to approaching traces (previous figure) which suggests that 10,000 PEO has not adsorbed to surfaces	71

Figure 25. 6,000 MW PEO, approaching surfaces. HF etched wafer, Si₃N₄ tip #3.
Addition of 6,000 MW PEO increases repulsion at low ionic strength 72

Figure 26. 6,000 MW PEO, approaching surfaces. HF etched wafer, Si₃N₄ tip #3.
Addition of 6,000 MW PEO increases repulsion at low ionic strength. . . . 73

Figure 27. 6,000 MW PEO, retracting surfaces. HF etched wafer, Si₃N₄ tip #3. Strong
adhesion is observed on retraction of the PEO samples 74

CHAPTER 1

INTRODUCTION

Background:

Two critically important aspects of integrated circuit manufacturing are wafer flatness and freedom from particulate (and other) contaminants. Ideally wafer surfaces are flat and smooth to optical dimensions. Particles as small as 160 nm can create circuit defects. At some points in the manufacturing process it is necessary to overcoat the incomplete mosaic of circuit elements with a thick coating of silica (amorphous SiO_2) and then to polish (abrade) away the top of the silica layer, regaining some degree of wafer smoothness. This polishing is achieved by lapping the wafers with a chemically active dispersion of colloidal silica particles - chem-mechanical polishing. These particles are necessary to achieve the polishing action, but they can cause defect generation if not completely removed before circuit processing continues.

Conventional particle removal techniques generally rely upon mechanical means such as sonication, centrifugation, and fluid displacement by liquid rinsing or blowing by a gas jet. These methods connote the evolution of IC technology. Only particles which are very large by today's standards (a few to tens of microns) were once considered destructive, and the conventional methods were effective. As the circuit technology has evolved, critical particle sizes have shrunk to the point of pushing limitations of these conventional cleaning techniques. Removal forces generated by these techniques do not scale proportionally with particle size-dependent adhesion forces. Consequently methods which exhibit sufficient leverage on relatively large particles become ineffective at removing very small particles. Many of the silica particles (and aggregates thereof) are larger than the current critical dimension of 160 nm, but remain within the domain of colloidal chemistry. This study seeks to exploit forces and phenomena commonly utilized in colloidal chemistry technology which determine the behavior of sub-micron particles.

Objectives and Overview

This study examines some practical applications of colloidal and surface chemistry in order *either* to PREVENT the adhesion of silica (SiO_2) silica particles to silica wafer-oxide layers *or* to REMOVE adherent dried silica particles from wafer surfaces. Planerization of wafer-oxide layers is achieved in current manufacturing processes by chemical-mechanical polishing of wafers with a slurry of silica particles. After polishing, wet slurry is removed by a combination of water rinsing and brush-scrubbing which is then followed by a drying step. These methods are not 100% effective at removing residual silica particles which results in possible generation of circuit defects.

This study can be divided into three objectives:

1. Investigate strategies for the removal of residual slurry which has been dried onto the wafer. Intel and OGI observations confirm that drying strengthens adhesion of silica particles.
2. Investigate the prevention of particle adhesion prior to initial drying through modifications of the rinsing process. Alterations of slurry prior to polishing are avoided in order to preserve present polishing process characteristics.
3. Direct measurement of forces generated between particles and wafers using an Atomic Force Microscope (AFM) in order to test a hypothesis based on macroscopic particle adhesion observations.

Studies conducted include:

1. Dissolution of residual silica particles, Chapter 4.1.
2. Vapor/Liquid interfacial displacement of particles from wafer surfaces, Chapter 4.2.
3. Utilization of surface-active agents in order to prevent particle adhesion, Chapter 4.3.
4. Direct measurements of adhesive forces, Chapter 5.

Summary of Results

Objective 1: Removal of dried adherent silica particles

- ☒ Either KOH or HF can be used to dissolve ~95% of silica particles without increasing wafer-oxide surface roughness (AFM measurements), page 28.

HF is faster : 10 min. vs. 5 hrs.

KOH sacrifices less wafer-oxide : 2 nm vs. 12 nm.

Objective 2: Prevention of particle deposition.

- ☒ Rinsing wafers with aqueous PEO (polyethyleneoxide) reduces residual particle counts by 90%. Remaining slurry is less tightly bound to the wafer. PEO residue is removed by standard industrial SC-1 and Piranha oxidative cleaning processes for organic contaminants, page 57.
- ☒ Fluid displacement of (wet) slurry by isopropanol was shown to reduce silica particle deposition on emersion from a rinse bath by 90%, page 38.
- ☒ Rinsing with high pH and low ionic strength solutions will maximize double layer repulsion between wafer surface and silica particles, pages 21 and 66.

Objective 3: AFM measurement of inter particle/wafer forces.

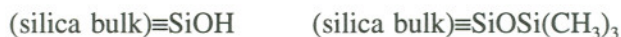
- ☒ An AFM was used to measure forces generated between silicon nitride particles and wafer-oxide surfaces in liquid environments, page 64.
- ☒ Ionic strength- and pH-force dependencies were consistent with double layer theory, and support rinsing at low ionic strength and high pH. These measurements illustrate the utility of this technique, page 66.
- ☒ PEO influences are observed but are not consistent with rinsing experiment observations. This is possibly due to AFM probe contamination, page 70.

CHAPTER 2

RELEVANT PRINCIPLES

This section briefly describes some relevant principles of surface and silica chemistry which influenced the directions of these investigations. Sources providing further details regarding surface chemistry^{1,2,3} and the chemistry of silica⁴ are included in the list of references.

The bond symbol "≡" which is normally used to indicate sp hybridized covalent triple bonds, will instead be used throughout this manuscript to represent the three single bonds connecting silicon atoms at the silica surface to three oxygens within the bulk amorphous SiO₂ network. The fourth bond indicates terminal groups of surface structure. Two examples of the latter are hydroxyl (also called silanol) and trimethylsiloxy surface terminations.



Surface Chemistry

Surface Tension: One important result of the ubiquitous intermolecular attractive forces is that work (energy) is required to create a surface from bulk substance. This can be expressed as either *surface energy* (energy per unit area, J/m² or more commonly ergs/cm²) or as *surface tension* (force per unit length, N/m or more commonly dyne/cm). These two forms are dimensional equivalents; the terms are synonymous. The surface tension of an interface is dependent on BOTH of the substances forming that interface (e.g. liquid and solid). Contaminants on a surface or in the fluid will alter the surface tension. Surface tension is commonly notated as $\gamma_{l,v}$, the subscripts denoting the two phases or compounds forming the interface (solid, liquid, vapor, compound).

Contact Angle: A drop of liquid on a solid surface creates an intersection of three interfaces - solid/liquid, liquid/air, and air/solid. The *contact angle* (θ , 0° to 180°) is defined as the angle between the solid/liquid and liquid/vapor phases, Figure 1. The contact angle is determined by the balance of the three interfacial surface tensions; in all cases Young's equation

holds true: $\gamma_{s,l} + \gamma_{l,v} \cos\theta = \gamma_{s,v}$. Driven by this dynamic equilibrium a droplet will expand or contract (Figure 1-A and B). Similarly, a meniscus will climb or drop relative to a stationary solid surface (Figure 1-C and D). If gravity and buoyancy are negligible (as for small particles) a particle will rise or fall relative to the interface until the inherent contact angle is established AND the fluid surface is level (Figure 1-E and F). This spontaneous adjustment of the three interfacial areas is driven by reduction of the net surface energy. The magnitude of the contact angle is dependent upon the same factors as is surface tension - most significantly: the identities of the three media, and the presence of any adsorbed substances (surfactants or contaminants) at the interfaces.

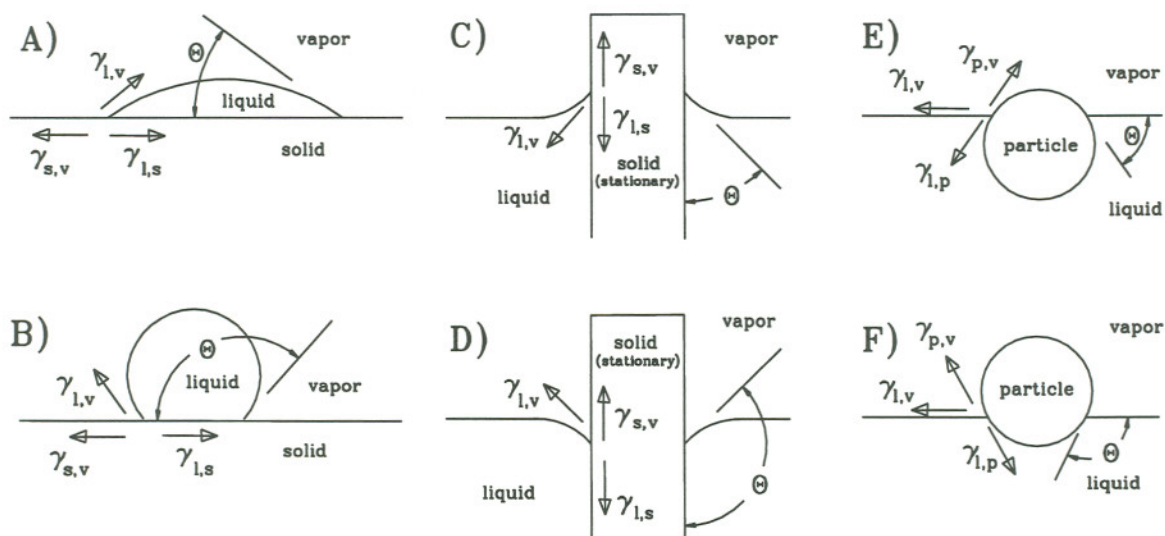


Figure 1. Contact angles (θ) and surface tensions (γ): A) Water droplet on a hydrophilic surface, B) Water droplet on a hydrophobic surface, C) Stationary hydrophilic surface at a water interface, D) Stationary hydrophobic surface at a water interface, E) Hydrophilic particle at a water interface, F) Hydrophobic particle at a water interface.

Component Forces Yielding Net Adhesion or Repulsion: Mutual adhesion or repulsion between two bodies is the net sum of several forces. These forces vary in magnitude, effective distance or decay length, and mechanistic origin. They are characteristic of the substances comprising the bodies and are influenced both by the geometry of the bodies and by the nature of intervening media. Thus, bodies which experience attraction at one separation distance can be repelled at other distances. Addition of an adsorbate to the surfaces can change an attractive

interaction to a repulsive one (or vice versa). Bodies attracted in one media can be repelled in another media. Even subtle changes of pH or ionic strength (salt concentration) in solution can shift mutual repulsion to attraction. The practical implication of this substance and media dependence is that rinsing processes need to be designed or optimized for specific particle and wafer materials. For example in the pH range between 2 and 7 silica in water acquires a negative surface charge, while silicon nitride in water supports a positive charge. In this pH range silica surfaces will repel one another, but silica surfaces will be attracted to silicon nitride surfaces.

i) Born repulsion: At separation distances of a few Ångstroms (the lower limits of the colloidal distance regime) contact between two bodies is limited by the resistance to electron-cloud overlap between the atoms of the two bodies. At this intimate contact (and barring particle deformation, inter-penetration by diffusion, or covalent bonding) the two bodies cannot be made to overlap due to this "hard-shell" repulsion of the surface atoms' outer-shell electrons, Figure 2.

ii) van der Waals Forces: Molecular and atomic (including permanent, instantaneous, and induced) dipole moment interactions are collectively referred to as van der Waals forces. They effect inter-atomic, inter-molecular, as well as inter-particle interactions. They are nearly always attractive and short ranged, often dominating the net interaction in the range of 0 to 5 nm, Figure 2.

iii) Electric Double Layer: When a solid surface is immersed in a suitable liquid (electrolyte), ionic species from the solid can diffuse into the liquid. Also, ionic species in the liquid can selectively adsorb onto the surface. In general, cations are enveloped by an associated layer of water while anions are less hydrated. Thus, hydrated cations are displaced farther from a surface than are anions. Specifically, the silica surface is rich in silanol groups ($\equiv\text{Si-OH}$, $\text{pK}_a \approx 6.8$)^{page 182 of reference 4} which deprotonate in aqueous media to yield a negatively charged siloxy anion surface ($\equiv\text{Si-O}^-$) below a cation-rich aqueous layer. The result is that a charge separation

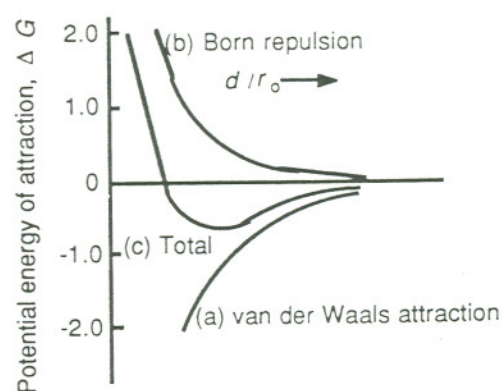


Figure 2. Net energy of interaction (curve "c") arising from the combination of Born repulsion (curve "b") and van der Waals attraction (curve "a"). Figure from page 59 of reference 3.

develops near the surface - the electric double layer. An analogy would be the formation of the depletion region at a PN junction. Compression of two immersed surfaces supporting charged double layers is then resisted by both electrostatic and osmotic forces. Thus the presence of an ionic double layer is an important component of inter-surface repulsion.

iv) Hydration force⁵ can be either attractive or repulsive. Both cases arise by virtue of several layers of highly organized water molecules which form on the two adjacent surfaces. The hydration layer is a network of water molecules associated by an extended series of hydrogen bonding. Structural Force and Solvation Force are terms synonymous to hydration force in the cases of nonaqueous solvents.

Attractive hydration forces are generated between hydrophobic surfaces, where associated water molecules' dipole orientations are more or less parallel to both surfaces. The attraction is driven by the (local decrease, but) overall increase in entropy gained as the structures of the two hydration shells unite. This attractive interaction is commonly called the "**hydrophobic interaction.**"

Repulsive hydration forces are generated between hydrophilic surfaces (silica is hydrophilic). This is a result of the anti-parallel orientation (opposing dipole moments) of the dipole moments in the two hydration layers (both perpendicular to their respective surfaces and opposing each other). It has been suggested that the repulsive phenomena be called the "**hydrophilic interaction.**"

Zeta Potential is an indirect measure of surface-charge and strength of the double layer, Figure 3. It is the potential difference between the bulk solution and the outer boundary of adsorbed counterions - the Shear plane.

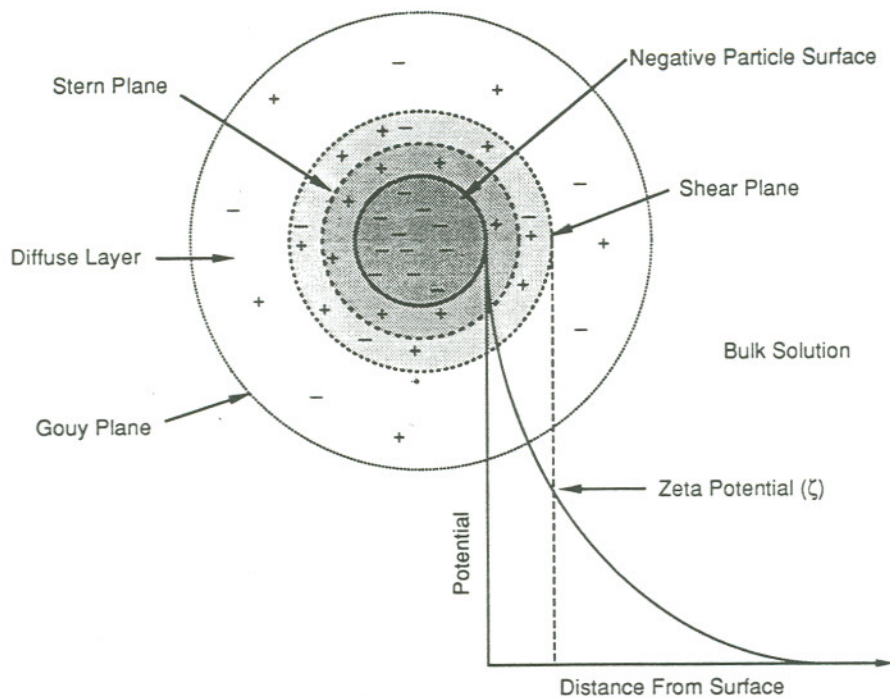


Figure 3. Zeta-potential and its relation to the double layer surrounding a negatively charged particle surface. The zeta-potential is the potential difference between bulk solution and the Shear plane. The Gouy, Shear, and Stern planes are the outer boundaries of regions of ionic distributions defined in the Gouy-Chapman-Stern-Grahme model of the electrical double layer. Within the Shear plane ions and counterions remain associated with the particle, while outside this plane ions diffuse freely through solution. Figure from reference 22

The **DLVO theory**^{6,7} approximates repulsive/attractive interactions in dilute solutions as a function of distance between two surfaces. It combines models of van der Waals and double layer interactions and generally predicts strong attractions at very close separations (<5 nm) and moderate repulsion at medium distances (5-50 nm) decaying to no interaction at large distances, Figure 4. The force/distance relationships are dependent upon many solution variables; the general prediction described above is by no means universal. The "medium range moderate repulsion," for example, can be obliterated by the addition of salt or a shift of pH rendering a once stable suspension unstable.

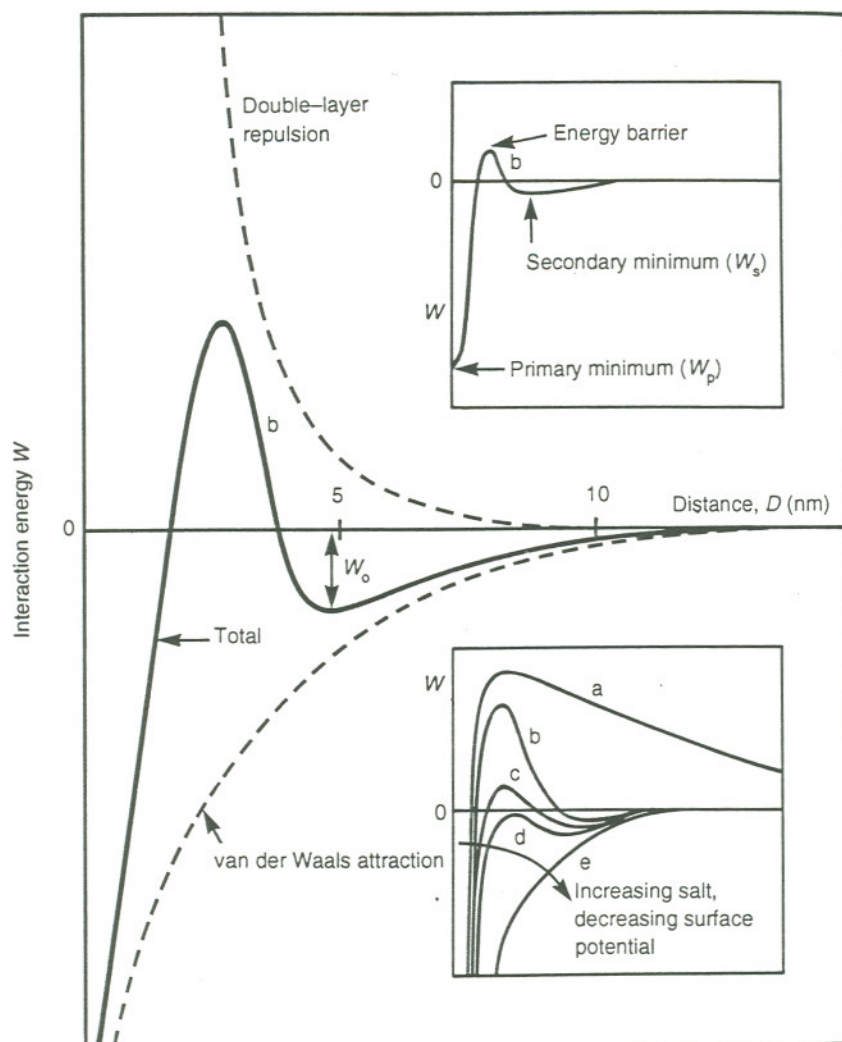


Figure 4. DLVO prediction of net interaction energy (solid line) versus separation distance arising from the combination of van der Waals attraction and double-layer repulsion (dashed lines). Lower inset shows the effect on increasing ionic strength which reduces the double-layer repulsion. Figure from page 248 of reference 1.

Modified DLVO theories incorporate adjustments to the DLVO model in order to either refine the modeling of the original forces (e.g. double layer⁸), or to account for additional forces contributing to the force/distance relationships. The inclusion of hydration force is one significant addition. This contributed to a better understanding of colloidal silica stability and the reconciling

of theory to experimental observations - notably, the observed stability of silica dispersions at the isoelectric point, where the classical DLVO theory predicts coagulation.

Adsorption: Ionic or molecular species can be attracted and bound either tightly (chemically) or loosely (physically) to a surface. This adsorption phenomenon can be exploited in order to alter the nature of a surface. Common examples are detergents which facilitate suspension of soils in water, and flocculants which destabilize silt (suspended water-borne particles) and thereby clarify the water.

Dispersion, aggregate, and floc are terms describing various states of particulate association in a fluid. Particles under the influence of effective mutual repulsion are suspended homogeneously in a fluid dispersion. Particles attracted to one another form small aggregates, which may remain suspended. Larger aggregates which fall out of suspension are called floc, the action flocculation. **Redispersion** is a condition arising from the exchange of one dispersion mechanism for another.

Silica Chemistry

Hydroxylated Silica Surfaces:

Surface siloxane bonds (Figure 5A) are readily hydrolyzed to form hydroxylated surfaces (Figure 5B.) Surface hydroxyls can be isolated, closely spaced (vicinal), or stem from the same silicon atom (geminal) if in aqueous media. Vicinal hydroxyls can hydrogen bond to one another if lacking water, or more likely, adsorb water through hydrogen bonding. A water molecule can bond to either an isolated hydroxyl or be shared by two vicinal hydroxyl groups. Water can bond oxygen down or up. The doubly bound water is held more tightly than the singly bound water (Figure 5C.) Deprotonation in aqueous solution and selective adsorption of ions from solution forms the double layer (Figure 5D.)

The extent of deprotonation, and consequently silica's ability to adsorb cationic surfactant (TMAH, CTAB) or to form hydrogen bonds with nonionic adsorbates (PEO, PVA) is dependent upon solution pH. The degree of deprotonation is essentially zero at pH 2 to 4, rises slightly through pH 7 (to 0.2 $-O/nm^2$) then steeply to pH 10.8 (to 1.1 $-O/nm^2$.) (In total there are 4.5 to 6 $-OH/nm^2$.)^{page 356 of ref. 4} At a given pH, increasing the salt concentration increases the population of deprotonated silanol sites.

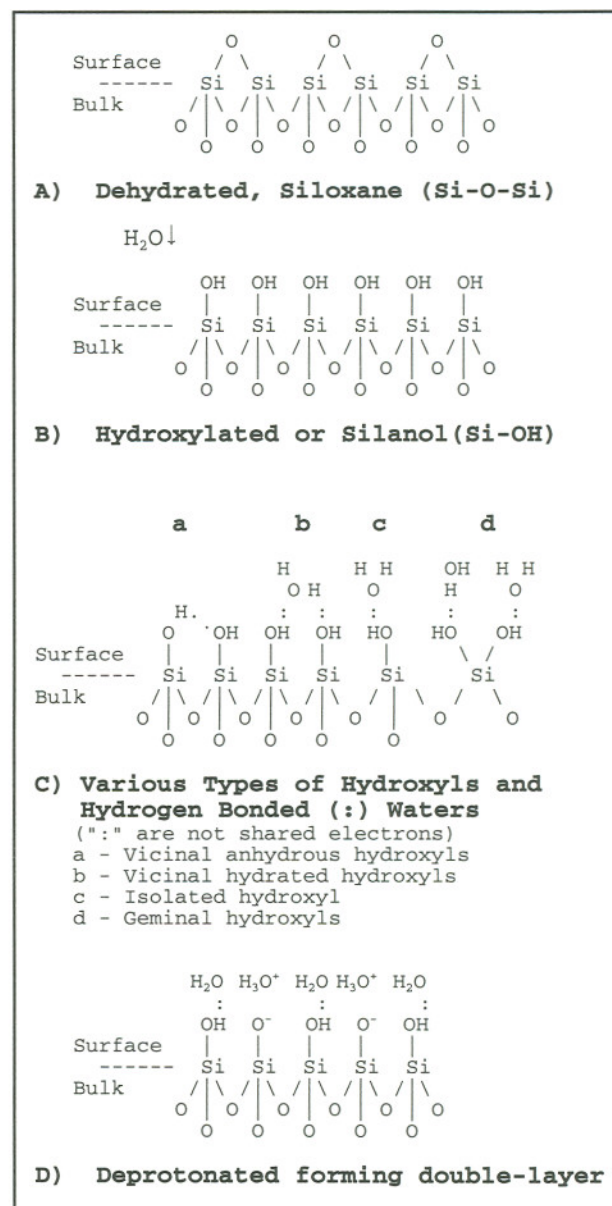


Figure 5. Various states of hydration and hydroxyl association. Silica being amorphous, the bulk "-O-" segments represent several -O-Si-O- segments and branches.

Thus the solution pH and ionic strength become important when considering adhesion modifications which rely upon adsorption of a surfactant or polymer.


Particle Bonding Mechanisms

At least six mechanisms can contribute to the adhesion between particles and larger (wafer) surfaces. Some are macroscopic extensions of the adhesive forces described above. Relative bond strengths are listed in Table 1.

van der Waals forces described above also cause particles and larger bodies to adhere to one another. The adhesive force due to van der Waals attraction (F_{vdw}) between a spherical particle and a flat surfaces is given by⁹ $F_{vdw}=AR6^{-1}D^{-2}$ where A is the Hamaker constant (0.65×10^{-20} J for silica^{page 273 of 2}), R is the particle radius, and D is the distance between the two. A value of 0.2 nm for D is used in the estimation of intimate contact distance.^{page 179 of 1}

Hydrogen Bonding forms between two surfaces in intimate contact if both contain complementary surface structure groups capable of forming hydrogen bonds.

Capillary Adhesion: Water has a higher affinity for silica than for air, thus thin films of water remain on "dry" hydrophilic silica surfaces. Driven by the reduction of surface free

energy, this water collects at the concave contact region (). One meniscus climbs up the particle surface, the other spreads laterally across the wafer surface in order to establish the characteristic contact angle of the system. The net result of the summed water surface tension being out of the plane of the wafer is the generation of adhesive forces compressing the particle into the wafer. Experimental measurements of water-capillary adhesive force (F_{cap}) between silica spherical particles and a flat surfaces in intimate contact (which yields maximum attraction) is closely approximated by^{page 332-333 of 1} $F_{cap}=4\pi R\gamma_L \cos\theta$ where R is the particle radius, γ_L is the water interfacial energy, and θ is the silica/water contact angle ($\sim 0^\circ$).

Hydrophobic Interaction: Hydrophobic surfaces immersed in water are drawn together as a result of the hydrophobic interaction described in the "Hydration Forces" section above.

Cationic Bridging occurs between two negative double layers via adsorbed multivalent cations or cationic polymer segments.

Silanol Condensation: A chemical pathway (silanol condensation, the reverse of silica hydrolysis) exists for the fusing of silica particles to wafer surfaces via strong covalent chemical bonds. These bonds are an order of magnitude stronger than the physical bonds (van der Waals and hydrogen bonding) generally responsible for initiating particle adhesion.



Both the act of drying and the concave geometry of the particle/wafer interface promote this reaction. Capillary adhesion compresses the particle into the wafer as the adhesive water film between them is lost. Concurrently, chemical equilibria in the water adhesive layer shift to favor the dehydration of the surface silanols and precipitation of dissolved silicate, fusing the two surfaces via covalent siloxane linkages. This condensation is thermodynamically biased in favor of locations at concave surfaces; in these regions silica solubility decreases relative to bulk solution (Figure 9, Page 28.) Consequently, the region at the particle/wafer interface fills in with new silica, in effect cementing the particle to the wafer. (It is somewhat ironic that this condensation is also thought to be partially responsible for the success of the polishing mechanism.¹⁰) This covalent attachment must be reversed to free the particle from the wafer surface. However, due to the indicated silica chemistry intrinsic in the wafer-oxide and bulk phase, selective dissolution of the Si-O-Si adhesive bonds without perturbing the wafer surface is difficult, as all three regions (particle, adhesive condensate, and wafer-oxide) are the same material - silica.

Table 1. Adhesive strengths of particle bonding mechanisms.

<u>Bond type</u>	<u>bond energy</u>	<u>Spherical Particle/Flat Plate Interactions at Intimate (0.2 nm separation) Contact</u>	
		<u>force on 100 nm radius particle</u>	<u>force normalized by particle radius, F/R</u>
van der Waals	N/A	2.7 nN	27 mN/m
Capillary Adhesion	N/A	92 nN	920 mN/m
Hydrophobic Interaction	N/A	-	200-400 mN/m
Hydrogen Bonding	10-50 kJ/mol	-	-
Covalent Si-O	370 kJ/mol	-	-

Liquid-Based Silica Particle Deposition Mechanisms - Entrainment

Deposition of particles onto wafers from an aqueous bath takes place by one of two mechanisms, depending on the relative signs of the particle and wafer zeta-potentials.¹¹ Particles charged oppositely of wafers are attracted by and accumulate gradually onto the wafer surface throughout the immersion period; apparently the deposition rate is diffusion limited. Distinctly different is the deposition of particles bearing the same charge as wafers; this takes place by an *entrainment* mechanism, Figure 6. This is the case for the silica particles and wafers; both bear negatively charged surfaces. While immersed, double-layer repulsion inhibits deposition of these particles. However, withdrawal of the wafer from the bath introduces the entrainment mechanism: the hydrophilic wafer collects a particle-laden wet film from the aqueous media. Subsequent evaporation of the film then is responsible for the deposition of the particles onto the wafer. In the cited study,¹¹ particle counts deposited by the entrainment mechanism were shown to be independent of immersion time, to be proportional to particle concentration in the media, to be proportional to the number of immersion/emersion cycles, and, within limits, to be proportional to emersion rate - fast withdrawals result in thick films and high particle counts, slow withdrawal enhances draining giving thin films and low particle counts.

The two slurry deposition techniques used for preparation of experimental samples described below incorporate the entrainment mechanism. Dip coating is simply emersion at a controlled rate. Spin coating causes recession and evaporation of the media from the wafer center outward. This mechanism requires that the wafer be wet by the dispersion media. Hydrophobization of the surface should reduce the reliability of this deposition. Further implications of this restriction are discussed in sections 4.2 and 4.3.

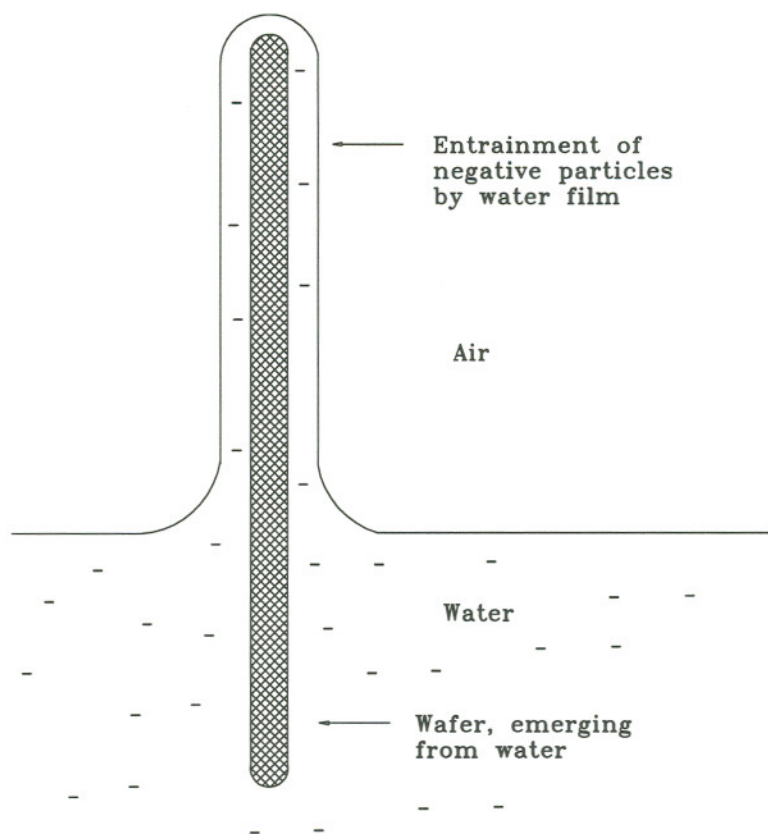


Figure 6. Entrainment of negatively charged particles. Suspended particles deposit onto a negatively charged hydrophilic wafer as the wetting water film evaporates after immersion.

CHAPTER 3

EXPERIMENTAL MATERIALS AND METHODS

In the wafer polishing process both the slurry and wafer silica surfaces have hydrophilic hydroxylated surfaces. This then is the baseline (control) condition to which experimentally modified surfaces are compared.

Most experiments seek to manipulate rinsing characteristics of the dispersion media and to weaken the adhesion strengths of the residual silica particles. Most surface modifications consist of the adsorption of water-soluble surface-active agents which are added to the aqueous slurry suspension media prior to particle deposition onto the wafer. Other modifications are chemical derivatizations of the surface hydroxyls in non-aqueous media yielding hydrophobic methylated silica surfaces. In both cases the modifications are intended to alter the physical and chemical bonding characteristics of the hydroxyl surface so as to inhibit the strong physisorption mechanisms otherwise promoted by the surface silanol. Many of these modifications also increase the hydrophobicity of the wafer surface, which impedes entrainment particle-deposition, thereby also improves rinsing.

These experiments share a similar methodology. Silica particles are deposited from various wet-suspension media and then are dried onto test wafers. Dried particles and aggregates are then counted in order to evaluate the rinsing quality of the deposition media - low counts indicate ineffective deposition which is equated with effective rinsing. Subsequent sonication of the particle-laden wafers and a second counting gives an indication of adhesion strengths of the dried particles - removal by sonication indicates weak adhesion while resistance to removal indicates strong adhesion.

Water

All water used was pre-treated by reverse osmosis and then filtered through a Millipore Milli-Q filter system which delivered 18 M Ω -cm water.

Test Wafers

4" diameter p-type (boron doped, 5 - 100 Ω ·cm) <100> silicon wafers with approximately 1150 Å of thermally grown SiO₂ were used as test substrates throughout these experiments.

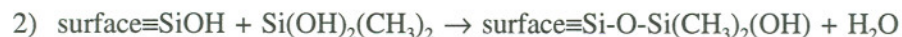
Hydroxylated (Hydrophilic) Test Wafers

Test wafers were rendered hydrophilic by immersion in 0.06 M KOH solution for 20 to 60 minutes, followed by rinsing and storage (0 - 2 hours) in water. This replicates the polishing process. These conditions facilitate hydrolysis of relatively hydrophobic surface siloxy bonds ($\equiv\text{Si-O-Si}\equiv$) to two hydrophobic silanol groups ($\equiv\text{Si-OH}$.) This hydroxylated silica wafer surface is the surface of primary interest in these studies.

Methylated (Hydrophobic) Test Wafers

Methylated surfaces were desirable in some cases, either for control of wafer hydrophobicity or for investigations comparing bonding mechanisms in relation to hydroxylated or methylated wafer surfaces.

Silanization of surface silanol by dichlorodimethylsilane ($\text{SiCl}_2(\text{CH}_3)_2$) (Aldrich, 99%) yields a dimethylchlorosilanized surface. The reaction below has been generally accepted,¹² but is currently the topic of some debate.^{13,14,15} Trace contaminant or adsorbed surface water is the source of the H₂O.



Silanizations were made in hexadecane solvent (Aldrich, 99%.) This reaction is slow in dilute solution, and the degree of silanization can be controlled by reagent concentration.¹⁶ Various concentrations (4 to 10,000 μM) were allowed to react at room temperature for 1 hour yielding wafers of varying degrees of silanization and resulting contact angles (Figure 7.) The hexadecane and reagent were then rinsed off in one of two ways: either 1) a series of methylene chloride, ethanol, acetone, and water rinses or 2) three sequential rinses in diethyl ether followed

by water. The first method was used in the Displacement of Wet Particles by Isopropanol experiment, the second in the Controlled Bonding experiment.

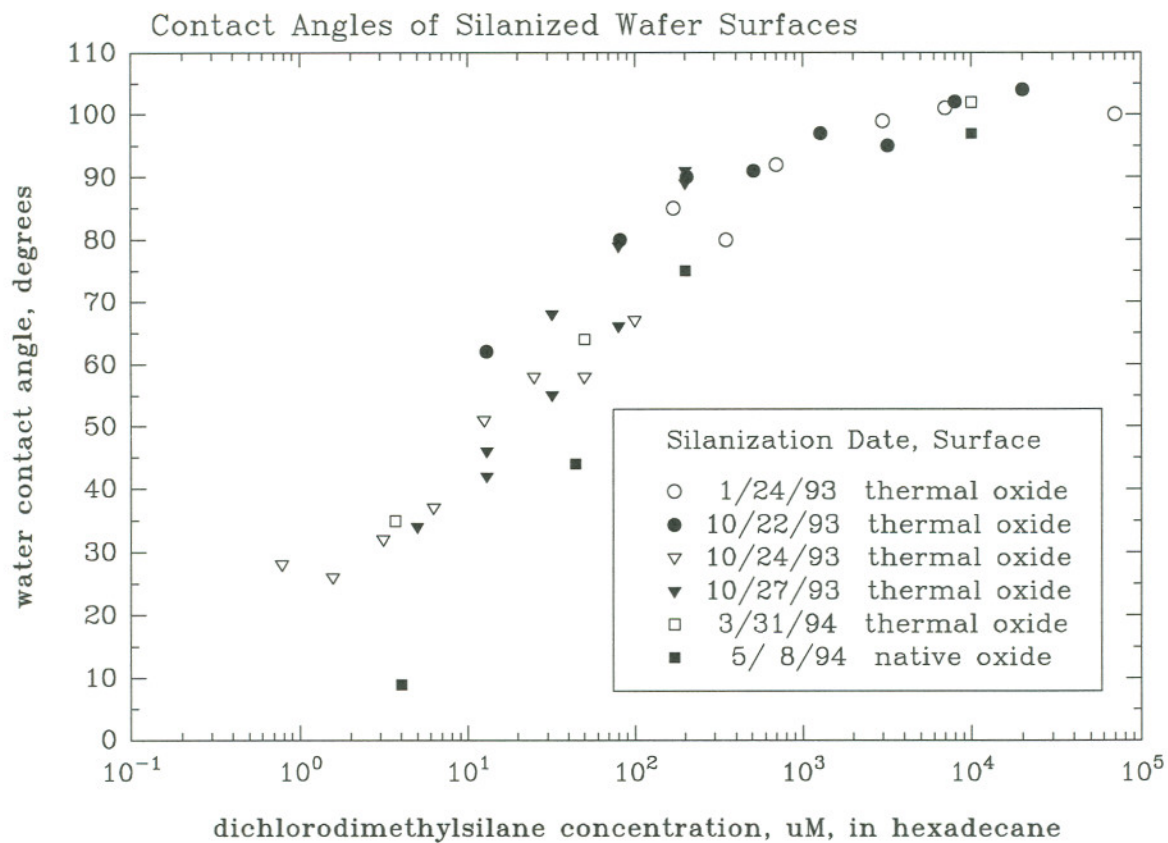


Figure 7. Contact angle of silanized wafer surfaces. Hydrophilic silica wafers were immersed in dilute dichlorodimethylsilane in hexadecane for one hour at room temperature. These data were collected from several separate silanization batches, the dates of syntheses are indicated. Thermal oxide samples are the ~ 1100 Å grown oxide surfaces used in these studies. Native (~ 20 Å) oxide samples are silicon wafers produced for another study.

SS-25 Slurry Characterization

This untreated fumed silica suspension is the slurry of primary interest in these investigations; it is characterized by a surface terminated with silanol groups, in contrast to the treated (methylated) TS-530 product which is described on page 21. Cabot Corporation's Semi-Sperse® 25 polishing slurry is a 25 wt% colloidal silica suspension in dilute aqueous potassium hydroxide solution. It is further diluted to 10 wt% silica for polishing applications.

In this text "SS-25" will be used to denote the 10 wt% silica concentration as supplied for this study. pH measurements of this concentration ranged from 10.6 to 10.7. SS-25 was usually diluted again for experimental purposes to 0.1 wt% silica, which is noted in this report as "1/100 SS-25." pH measurements of this concentration ranged from 10.2 to 10.6.

Repulsive double layer and hydrophilic (repulsive) hydration forces are responsible for the suspension's stability; the former dominates at the extremes of pH, the latter mechanism dominates near the pH 2 isoelectric point. Neither mechanism is very strong near pH 6 - 7, resulting in

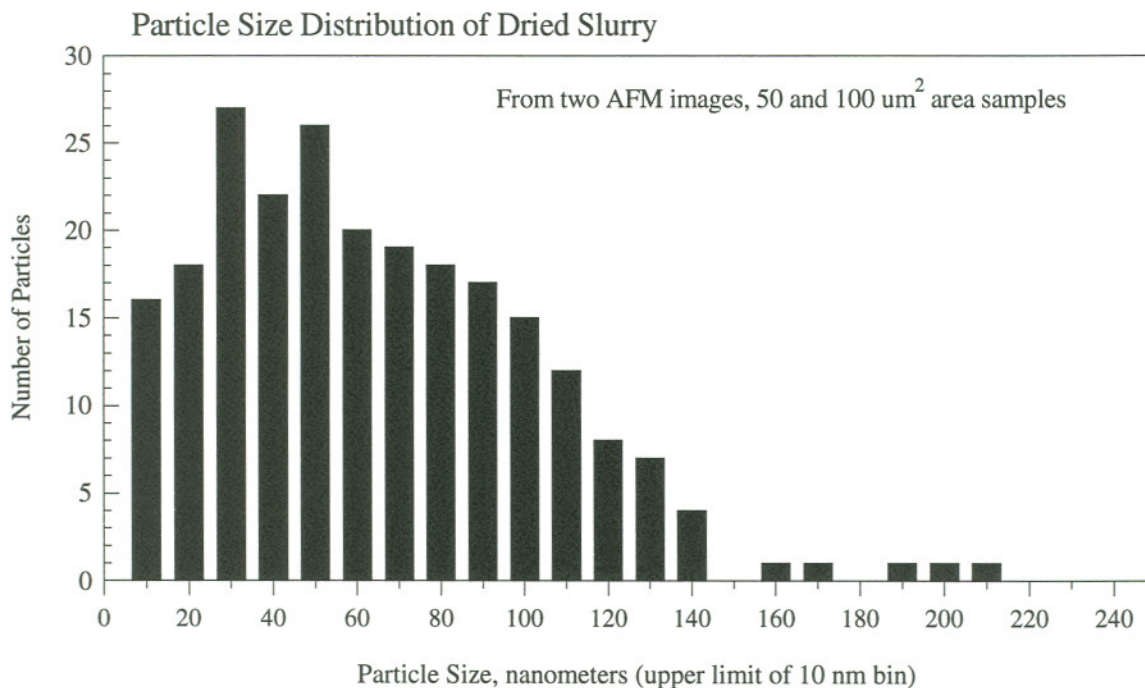


Figure 8. Particle size distribution of dried slurry. Particle size is determined from AFM images of dried particles deposited from 1/100 SS-25. "Size" is taken to be particle height above wafer surface and may be an underestimate as it does not reflect particle width. Structure of aggregates are often flake-like, lying broader than tall.

minimum stability in that region.^{17,18}

Cabot reports¹⁹ that silica particles are 7 to 35 nm diameter pyrogenic silica spheres which align in solution to form small aggregates or chains of up to 200 nm diameter or chain length. Intel's AFM measurements of dried silica particle residue show that particles and aggregates range from 5 to 200 nm, Figure 8. These samples were prepared by spin-coating deposition of 1/100 SS-25 slurry onto hydrophilic test wafers. The AFM imaging equipment is described on page 25. Particle size in these measurements were determined from the topological image produced by the AFM; particle size was taken to be the apparent elevation of the particle above the wafer surface. These data are from a very small sample: two wafers and 150 μm^2 total area. Observations using optical microscopy (3750 μm^2 per view) show occasional aggregates of slurry approaching 1 μm diameter. Aggregates in these AFM and optical samples may be an artifact of drying and not representative of dispersion conditions.

Cabot reports a measured surface area of 90 m^2/gram silica, yielding a nominal particle diameter of 30 nm. Useful physical and chemical quantities are calculated from this value in Table 2. Comparison to wafer area is enlightening. One milliliter of 1/100 SS-25 (polishing concentration) slurry has the same amount of silica surface area as 143 8" diameter silicon wafers!

Table 2. Physical and Chemical Quantities

Based upon nominal 30 nm diameter particles

Individual Particles (anhydrous)

particle diameter	30 nm
particle area	2,800 nm^2
particle volume	14,000 nm^3
particle weight	3.1E-17 g
# of Si atoms across particle diam.	84
Surface area per gram silica	91 m^2g^{-1}

Surface Hydroxyl (-OH) Concentration*

# of surface -OH per particle	22,000
mole of surface -OH per particle	3.6E-20
surface -OH per nm^2	7.7 nm^{-2}

Aqueous Slurry Dispersion Concentration Values*

	<u>SS-25</u> <u>10 wt% silica</u>	<u>1/100 SS-25</u> <u>0.1 wt% silica</u>
particles per liter	3.2E+18 l^{-1}	3.2E+16 l^{-1}
area per liter	9,100 m^2l^{-1}	91 m^2l^{-1}
surface -OH conc.	0.12 M	0.0012 M

* These values are calculated using one -OH per surface Si atom (7.7 nm^{-2}). Reported measured values range from 6 to 4.5 nm^{-2} . The hydroxyl density decreases with dehydration and particle size, and increases with pH.

SS-25 Slurry Zeta-Potential Measurements

Measured zeta-potential values of SS-25, as well as pH and ionic strength dependence (Table 3) are qualitatively consistent with theoretical expectation and published values.²⁰ Zeta-potential measurements of wafers were not made, but being of the same material, they are expected to show a similar trends. The behavior supports a rinsing strategy of high pH (>8) and low ionic strength in order to exploit the particle-wafer and inter-particle double layer repulsion which fortifies suspension stability and thus facilitates effective rinsing.

Zeta-potential values are calculated from electrophoretic mobility measurements collected with a Coulter® Delsa 440 multi-angle electrophoretic light scattering (ELS) particle analyzer.^{21,22}

Table 3. Zeta-potential of 1/100 SS-25 in phosphate/citrate/borate buffer.

pH	KCl (M)	Ionic Strength	Zeta-Potential (mV)
5.6	0.01	0.018	-22.4 ± 1.2
7.0	0.01	0.024	-35.3 ± 1.1
8.0	0.01	0.027	-47.4 ± 1.3
9.0	0.01	0.028	-52.5 ± 1.3
10.0	0.01	0.028	-50.8 ± 1.6
10.9	0.01	0.029	-54.0 ± 2.4
10	0.00	0.018	-59.1 ± 2.2
10	0.01	0.028	-57.0 ± 1.4
10	0.03	0.048	-55.1 ± 0.6
10	0.10	0.118	-48.6 ± 0.7
10	0.30	0.318	-38.4 ± 0.8

TS-530 Methylated Silica Slurry

Some experiments explore the effects of slurry surface compositions. Specifically, a comparison between hydroxylated and methylated silica is made. Cab-O-Sil® TS-530 (Cabot Corporation) is created by treatment of fumed silica with hexamethyldisilazane (HMDS) yielding a trimethylsilyl modified surface: $\equiv\text{Si-O-Si}(\text{CH}_3)_3$. Cabot reports a surface area of $325 \pm 25 \text{ m}^2/\text{g}$, which yields (assumed spherical) particle diameters of 8 to 9 nm. This hydrophobic silica was dispersed in either isopropanol or 50 v/v% isopropanol:water mixtures, then deposited and dried onto test wafers. This generated aggregate sizes both larger and more variable than did the aqueous 1/100 SS-25; the TS-530 aggregates ranged from roughly 1 to 20 μm diameter.

Contact Angle Measurements

Contact angle measurements were made by analyzing sessile drops (1-2 μl) on $\sim 2 \text{ cm}^2$ wafer fragments using a Ramé-Hart goniometer.

Suspension Stability Determination

Suspension stability was evaluated by visual observation of slurry in 1 cm diameter 7 ml glass vials. Instability was evident by gradual gravitational segregation of the suspension into upper clear and lower opaque phases, the latter containing the silica sediment. Segregation duration varied from seconds to hours depending on solution conditions. Under some experimental conditions suspensions remained "stable" (did not segregate) by this evaluation despite visible flocculation.

Slurry and Wafer Treatments

In actual practice, any surfactant added as a rinsing agent in the post-polishing rinse will be introduced *after* slurry has had an opportunity to contact and adhere to the wafer. In a conservative experimental approach it is desirable to allow surfactant adsorption to both slurry and wafer *before* giving slurry the opportunity to adhere to the wafer. In light of this dilemma two experimental treatments were used.

In **Separate-Treatment** trials, wafers and slurry were treated with surfactant in separate vessels *prior* to introduction of slurry to wafer. It is not incumbent upon the surfactant to break any preformed bonds (chemical or physical), only to prevent their formation. In **Combined-Treatment** trials, slurry and wafer were treated with surfactant together simultaneously in the same beaker, many minutes *after* the introduction of slurry to wafer. This requires the surfactant to work its way between possibly adherent particles and wafers.

Separate Treatment trials were conducted for all surfactants in order to demonstrate the ability to enhance rinsing or reduce adhesion. If so demonstrated, then Combined Treatment trials were performed in order to show the possibility of practical application. It should be noted that the temperature and pressures of the actual polishing process probably facilitates more particle adhesion than the Combined Treatment does. The Combined Treatment places the wafer face up at the bottom of a beaker filled with slurry prior to the addition of surfactant.

Silica Particle Deposition

Silica particles were deposited from dilute slurry onto wafers by one of two methods. Spin coating was used for all experiments except IPA displacement of wet slurry, for which dip coating was used. Both methods rely upon entrainment. Spin coating utilizes centrifugal

acceleration while dip coating uses gravitational acceleration to form the wet film of dilute slurry on the wafer.

Spin Coating: 3.0 ml of 1/100 Intel stock SS-25 (0.1 wt% silica) was deposited onto stationary wafers, and usually spread spontaneously and evenly across the wafer. Some experimental conditions yielded hydrophobic wafers which resisted this stationary wetting. In such cases spreading was accomplished by slow spinning at 140 rpm and/or by gentle persuasion using a low pressure nitrogen jet. After spreading, the wafer sat stationary for 1 minute to allow for any settling or adhesion to occur. This was followed by fast spinning at 285 rpm coupled with a pressurized nitrogen jet blowing from the wafer center radially outward was used to dry both the wafer and the deposited slurry. When using unmodified 1/100 SS-25 slurry and wafers this method yielded fairly uniform, homogenous and repeatable densities of deposited silica particles - 200 to 400 particles per 50x75 μm field. This then is the control baseline count and appearance against which experimental trials were compared.

Dip Coating: Uniform and repeatable baseline deposition characteristics were also produced by the slow emergence of a vertical wafer from an aqueous suspension of 1/100 SS-25. Within limits, particle density can be controlled by emersion rate, 0.01 cm/min yielding about 40 particles per 50x75 μm field. Emersion counts from this bath are the control baseline for the wet slurry/IPA interfacial displacement experiment.

Rinsing Enhancement

Repeatable deviation from spin-coating baseline particle counts and characteristics (described above) resulted from some of the various experimental treatments. These particle density decreases from the baseline value were interpreted as indicating improved rinsing.

Particle Counting Techniques

Tencor Surfscan model 4500: Calibration trials with this automated particle counter showed that the machine is incapable of quantitative detection of the silica particles. This machine detects and counts particles larger than about 300 nm diameter. Thus only the largest aggregates of slurry would be accurately "counted." Nearly all silica particles are below 200 nm (Figure 8.) Particles of this size are in a range of non-linear response resulting both from the nature of the small particle reflection (Rayleigh scattering) and to interfering reflections from the

wafer-oxide layer. Intensity signals from this range are lumped in a "haze" category and are indistinguishable from wafer roughness. The value of the haze reading does not absolutely portray small particle density. Particles in the countable size range were generally not slurry but dust particles - noise in the context of these slurry experiments. For these reasons automated counting was not employed in these studies.

Optical Microscopy: Silica particles were detectable and identifiable using optical differential interference contrast (Nomarski) microscopy at 800x magnification. The lower limit of detection is reported to be about 220 nm wide features. Particle appearance ranged from barely discernible to easily discernible. It is likely that many smaller particles were invisible. Particle counts reported in this report are the number of particles visible in a reticle rectangle of 50 x 75 μm . Generally five or six field counts per wafer were made.

Qualitative Nature of "Statistics": Optical microscope counts range from zero to thousands per field, counts greater than 100 are approximate and qualitative. Unmodified (control) and many treated samples yielded rather characteristic, uniform, and diffuse depositions of particles or small ($< 1 \mu\text{m}$) aggregates in the range of 400 particles per field; these were ascribed a particle count value of 400. Often, large aggregates or floc (10 to 50 μm), or very dense particle depositions were observed; a value of 1000 per field was ascribed to these. Observations of low particle densities (fewer than 100) were counted absolutely; and moderate densities (100 to 400 per field) were estimated based on counts from smaller, representative areas.

Due to the qualitative and categorical nature of the larger counts, statistical inference of all but the largest differences between sample groups is meaningless. Standard deviation values are presented in the data tables but are to be taken lightly. Many sample groups yield standard deviation values of "zero." These result from the categorical nature of the measurement where all measurements fell into the same qualitative bin assignment of either "400" or "1000." Standard deviation values of zero accompanying averages of zero are genuine.

Groups with average particle counts between 400 and 1000 and large standard deviations generally contain some floc; increasing average and decreasing deviation imply more floc, large aggregates, or thick particle depositions. Averages near 400 with small or "zero" deviation indicate normal control-like depositions. Averages below 400 suggest some improvement in rinsing (pre-sonication) or weaker adhesion (post-sonication data), with confidence improving with

decreasing average and standard deviation. Calculations of confidence intervals and other statistical treatments would be grossly misleading.

Atomic Force Microscopy Imaging was used to measure particle size, deposition density, and wafer roughness in the slurry dissolution experiments. The microscope is a Digital Instruments Nanoscope III, using non-contact tapping-mode. The probes are manufactured by Nanosensors (Germany) and distributed by Digital Instruments. The etched silicon cantilevers have nominal (as reported by the manufacturer) cantilever force constants of 34 to 56 N/m, and a resonant frequency of 170 to 190 kHz. 10 μ m by 10 μ m images were collected at 0.8 Hz lateral scan rate.

Adhesion Force Measurements

A primary objective of this investigation was to quantify net adhesive forces and to show reduction of net adhesive force as a result of experimental treatment. Direct measurement is possible (see AFM, below) but impractical for large samples. Access to an AFM was limited to a single week, restricting the scope of direct measurement to a single adhesion-reduction treatment. Lacking full access to an AFM, an indirect method using sonication was used to compare relative magnitude of adhesive forces for most experimental treatments.

Sonication (ultra-sonic cleaning) was used to determine relative adhesive strengths between treated (experimental) and untreated (control) slurry on wafer samples. If sonication removed dried treated slurry but did not remove the untreated control sample, then the treated sample was presumed to be less adherent. Particle removal by sonication relies upon cavitation. Microscopic, transient cavities of vapor are generated within the fluid at anti-nodes of sonic energy. Implosion of these cavities generate shock-waves which propagate through the medium, dislodging particles from surfaces. Cavitation intensity varies for different fluids: water is relatively high while isopropanol is rated at 38% of water's intensity.²³

In these experiments it was found that sonication in water sometimes removed dried control slurry *as well as* experimentally treated slurry, thereby eliminating any means for comparison between the two. Sonication in IPA, on the other hand, did not remove control particles but did remove some treated particles. Therefore IPA was chosen as the test fluid, enabling a qualitative estimation of relative adhesion strength between treated and untreated slurry residues.

(Sonication at ultra-sonic frequencies has been shown to cause destruction of circuit features and so is not considered a manufacturing-worthy solution for removal of silica particles.)

Admittedly, there is a flaw in this logic. Cavitation is also dependent upon surface wettability. Non-wetted particles shrouded by tiny bubbles would not receive the full force of the fluid's shock-wave. It is conceivable that the removal of treated particles is attributable to better wetting of treated surfaces by IPA. The resulting enhanced cavitation, rather than reduced adhesion, then would explain the removal of treated slurry.

The sonication bath is a 1 gallon Branson D-150, 55 kHz unit filled with water and a few ml of Micro laboratory detergent. Into this bath was suspended a beaker filled with IPA and the sample wafers supported horizontally in an abbreviated (9 slot) wafer cassette. Sonication duration was 20 minutes with sample repositioning every five minutes in order to distribute "hot spot" (anti-node) exposure. IPA temperature rose from about 23°C to about 35°C over the duration of sonication.

Direct Force Measurements Using AFM: Atomic Force Microscopy (AFM) is commonly used to generate nanometer scale topographical images of surfaces. Alternative configurations of the apparatus and signal processing facilitates direct measurement of forces between stylus and substrate as a function of separation distance between the two. Measurement can be made in a fluid. In this configuration the effects of solution variables on the force/distance relationship of two surfaces can be measured quantitatively: resolutions of nano-Newtons and nanometers are common.

This study made use of a Digital Instruments Nanoscope III with a fluid cell. The silica test surfaces were ~1 cm² segments of the test-wafers provided by Intel ("Test Wafers", page 17.) The AFM probes used are manufactured by Nanosensors (Germany) and distributed by Digital Instruments. Their etched silicon cantilevers are "V" shaped; the calculated spring constants for the three probes used are 0.14, 0.18, and 0.18 N/m. The radii of the rounded tip of the 3600 nm tall pyramidal silica nitride styli were about 40, 50, and 80 nm. These are the radii used to calculate the Force/Radius values.

The probe's silica nitride stylus is used to represent the silica particle. This a reasonable substitution for high pH environments. The silicon nitride pzc is pH 6.8 and the silica pzc = pH 2, both surfaces bear silanol groups, which are largely deprotonated at high pH.

CHAPTER 4

EXPERIMENTAL INVESTIGATIONS

Experimental investigations are broken into four groups according to their objectives. In the first set (Chapter 4.1) untreated dried residual silica particles are removed by dissolution. The second and third sets of experiments uses passage through a fluid interfaces in attempts to remove these dried particles (Chapter 4.2), or at least prevent their deposition from slurry dispersion (Chapter 4.3). The fourth set (Chapter 4.4) investigates the effects of aqueous surface-active agents on rinsing and particle adhesion strength. The principles, terminology, and methodology discussed in Chapter 4 are described in Chapters 2 and 3. In many cases cross-referencing is provided.

4.1 Dissolution of Adhered Particles

Dissolution by either HF or KOH etchant can be used to remove dried residual silica particles. Particles dissolve faster than planar wafer-oxide layers for both geometric and thermodynamic reasons. Geometrically, a particle on a surface loses material from its top and sides, while the surface (having no sides) retreats from the top only. Succinctly put: dissolution rates increase with increasing surface area (decreasing particle size.) Surface curvature has an effect on the thermodynamic activity of a substance, consequently solubility of small (concave) particles is increased relative to flat surfaces of the same material.²⁴ Likewise, solubility of the material within a small cavity is decreased, Figure 9. Thus at equilibrium, cavities will fill with condensate at the expense of dissolution of protuberances; and small particles will dissolve while large particles grow (Ostwald ripening.) These effects are most pronounced for silica particles smaller than 5 nm radius. page 51 of ref. 4

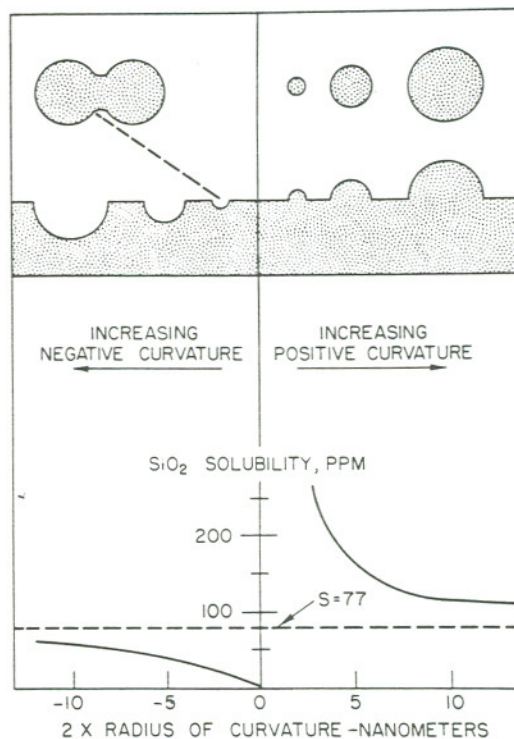


Figure 9. "Variation in solubility of silica with radius of curvature of surface. The positive radii of curvature are shown in cross section as particles and projections from a silica surface. Negative radii are shown as depressions or holes in the silica surface, and the crevice between two particles." Figure and caption from page 50 of reference 4.

Initial reservations regarding the utility of dissolution were that too much wafer oxide would be sacrificed and that mesas would form in the wafer oxide below the particles yielding unacceptably rough surfaces. Neither of these liabilities materialized in the experimental evaluations. Dilute HF dissolves residual silica particles much faster than KOH, but at the expense of six times more wafer oxide.

Samples for both HF and KOH experiments were prepared by spin coating 1/100 SS-25 slurry onto hydrophilic test wafers (pages 17 and 23). Etching was done at room temperature with minimal stirring.

Etch rates of wafer (thermal) oxide layers were determined by ellipsometry. Atomic force microscope images were used to measure silica particle size and wafer roughness for increasing etch periods. The difference in initial particle count/area between the HF and KOH samples (1.2 vs. 2.3 μm^{-2}) most likely is due to the small sample size (100 and 50 μm^2) and non-uniformity of particle depositions. This difference is considered to be insignificant, more likely a sampling anomaly rather than representative of two differing populations. The significant result is that both cases show approximately 95% reduction in particle density and approximately 85% reduction in particle size without an appreciable increase in wafer roughness.

Etch Summary	<u>0.14M HF</u>	<u>1.0M KOH</u>
Time to dissolve slurry :	10 min.	5 hrs.
Initial / Final particle size :	70 nm / 10 nm	50 nm / 5 nm
Initial / Final particle count/area :	1.2 μm^{-2} / 0.05 μm^{-2}	2.3 μm^{-2} / 0.15 μm^{-2}
Thermal wafer-oxide etch rate :	1.1 nm/min.	0.06 nm/min.
Thermal wafer-oxide lost in etch time :	12 nm	2 nm
Initial / Final rms surface roughness :	1.8 Å / 1.7 Å	1.8 Å / 2.4 Å

Dissolution in HF

Hydrofluoric acid is commonly used to dissolve oxide layers. Commercial sources are often buffered and augmented by surfactants; the HF solution used in this study was neither. Wafer oxide etch rate data are presented in Figure 10. Time dependent slurry size and density are presented in Figure 12.

Roughness data were collected in order to detect mesas which were suspected of being generated below silica particles as the etch progressed (Figure 12.) Roughness data are divided into three groups. "Slurryless sample" is a wafer which had no slurry deposited prior to etching. It serves as a baseline and shows the degree of roughening due to etching only, without being compounded by any slurry effects. "Including slurry" is the total roughness of another wafer surface which had dilute (1/100) SS-25 slurry deposited and dried onto it prior to the etch. It includes 100% of the sampled area including any remaining unetched slurry; it serves to show relative roughness values arising from the presence of obvious slurry. "Excluding slurry" is taken from the same sample areas as "including slurry," but any obvious remaining particles were

omitted from the roughness calculation. If mesas were formed, it was expected that the "including slurry" roughness value would remain above the "slurryless" baseline value for all etch times, and that particle (mesa) density would remain near initial values; mesas would simply replace their precursor particles. However, it was observed that the "including" and "slurryless" data do converge, which suggested that detectable mesas were not formed.

It should be noted that the constant-contact AFM head was used to collect the "slurryless" data while the tapping mode head was used for the "including" and "excluding" samples. The tapping-mode gives better resolution but was unavailable in the early stages of this experiment. The constant-contact head's higher noise level may account for the apparently rougher "slurryless" sample values.

Dissolution in KOH

The Potassium Hydroxide trials parallel the HF format. Wafer (thermal) oxide etch rate data is presented in Figure 11, wafer roughness and slurry dissolution in Figure 13. Etching was performed at room temperature with minimal stirring. Increasing temperature and KOH concentration would increase the etch rate, reducing the end-point time from the impractical duration of five hours for these experiments.

Like HF, AFM surface roughness data for KOH show that slurry-inclusive measurements converge with slurry-exclusive measurements, and that both are slightly smoother than slurryless samples. This, combined with the decreasing particle (or mesa) density, suggest that detectable mesas are not formed below silica particles.

1.0 M KOH (pH 14) was shown to dissolve only about 2 nm of wafer (thermal) oxide in the time required to dissolve silica particles (HF lost 12 nm.) Suspension of silica particles by double layer repulsion may explain KOH's higher ratio of particle to wafer-oxide etch rate in comparison to HF's.

0.14 M (200:1 v:v) HF Etch

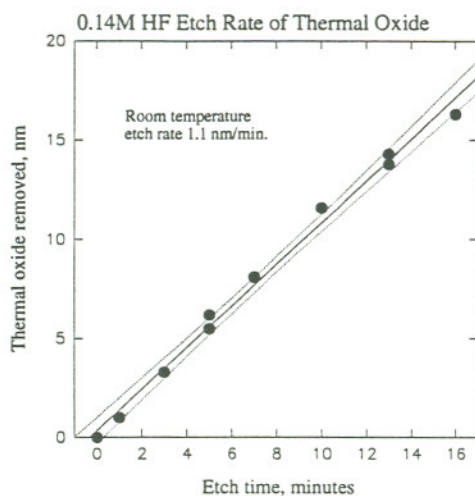


Figure 10. Wafer-oxide etch rate (solid) & 95% confidence interval (dotted): 1.1 nm/min.

1.0 M (pH 14) KOH Etch

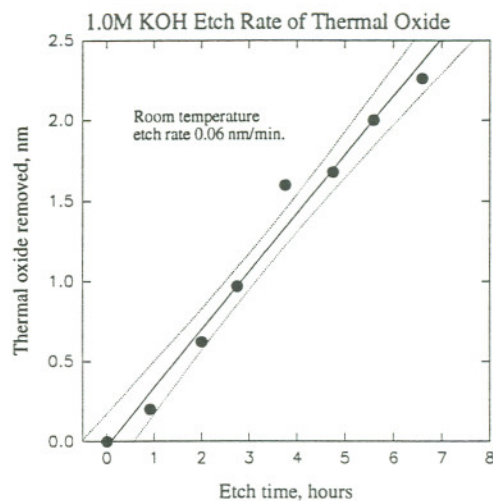


Figure 11. Wafer-oxide etch rate (solid) & 95% confidence interval (dotted): 0.06 nm/min.

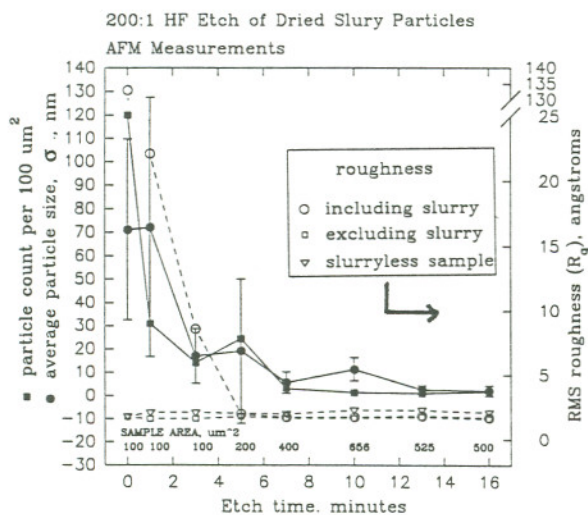


Figure 12. Left abscissa: particle count/area (\blacksquare), average particle size and standard deviation (\bullet and bars). Right abscissa: wafer roughness (\circ, \square, ∇). About 95 % of the initial particles are removed within 10 minutes. Mesa formation is not evident in surface roughness measurements.

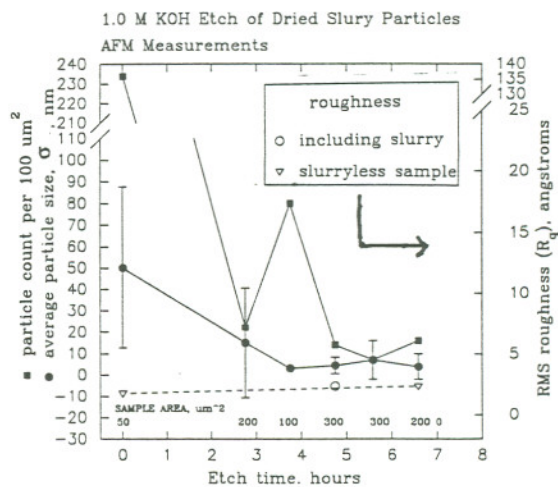


Figure 13. Left abscissa: particle count/area (\blacksquare), average particle size and standard deviation (\bullet and bars). Right abscissa: wafer roughness (\circ, ∇). About 95 % of the initial particles are removed within 5 hours. Mesa formation is not evident in surface roughness measurements.

4.2 Extraction of Particles by Passage Through A Fluid Interface

Most adhesive forces are directly proportional to particle radius, but the conventional removal forces scale by the square or cube of the particle radius. Thus, conventional particle removal techniques become less effective as particle size diminishes. The extraction force exerted upon a particle during passage through fluid interface, on the other hand, IS directly proportional to particle radius. Its leverage (ratio of adhesion to extraction forces) is independent of particle size. In theory, this is an enticing mechanism for removal of small particles.

A.F.M. Leenaars has developed a model for forces acting on a particle stuck to a wafer as the vertical wafer emerges through a fluid (e.g. water/air) interface.²⁵ Using this method he reports the removal of about 70% of the 700 nm diameter silica particles stuck to silicon wafers. In this section we unsuccessfully attempt to replicate his results, removing the smaller dried adherent silica particles from oxidized wafers.

Mechanism and Rationale

The following is a synopsis of the model presented by Leenaars.²⁵ Figure 14 shows three cases of a spherical particle straddling a liquid/vapor interface. The position of the particle relative to the triple-phase circle (the solid/liquid/vapor intersection circumscribing the sphere) can be described by the angle ϕ (similar to the global parallels of latitude, but referenced from 0° at the North Pole rather than at the Equator.) For particles smaller than about $10\ \mu\text{m}$, gravitational, buoyant, and hydrostatic forces are negligible in comparison to the surface tension forces acting on the particle. A small spherical particle (Figure 14 B) will straddle a fluid interface at a position of equilibrium (ϕ) determined by the particle contact angle (θ), which in turn is determined by the surface tensions of the three interfaces ($\gamma_{l,v}$, $\gamma_{l,p}$, $\gamma_{p,v}$.) In this equilibrium position $\phi_{\text{Eq}} = \theta$, the liquid surface will be flat, and $\gamma_{l,v}$ will be parallel to it. Displacement of the particle up (Figure 14 A) or down (Figure 14 C) by some hypothetical test force (F_H) will result in the generation of a restoration force (F_R) which attempts to push the particle back to the equilibrium position. This restoration force arises from the distortion of the fluid surface (meniscus) with the displacement of the particle. The meniscus forms because the liquid/particle contact angle (θ) remains constant, despite particle displacement relative to the fluid surface. The formation of the concave meniscus (Figure 14 A) or convex meniscus (Figure 14 B) skews the

surface tension vector $\gamma_{l,v}$ out of plane of the fluid interface. Integration of the vertical component of this surface tension about the triple-phase circle yields the restoration force (F_R) acting to return the particle to the equilibrium position.

$$\text{Restoration Force} \quad F_R = 2\pi R \gamma_{l,v} \sin \phi \sin (\theta - \phi)$$

With ideal combinations of wafer contact angle (α), θ and ϕ this restoration force can counteract particle/wafer adhesion forces and thus be exploited to pull particles from wafers by passing the wafers through a liquid/air interface. With non-ideal combinations of α , θ and ϕ the restoration force will reinforce the adhesion, compressing the particle into the wafer by a variation of capillary adhesion.

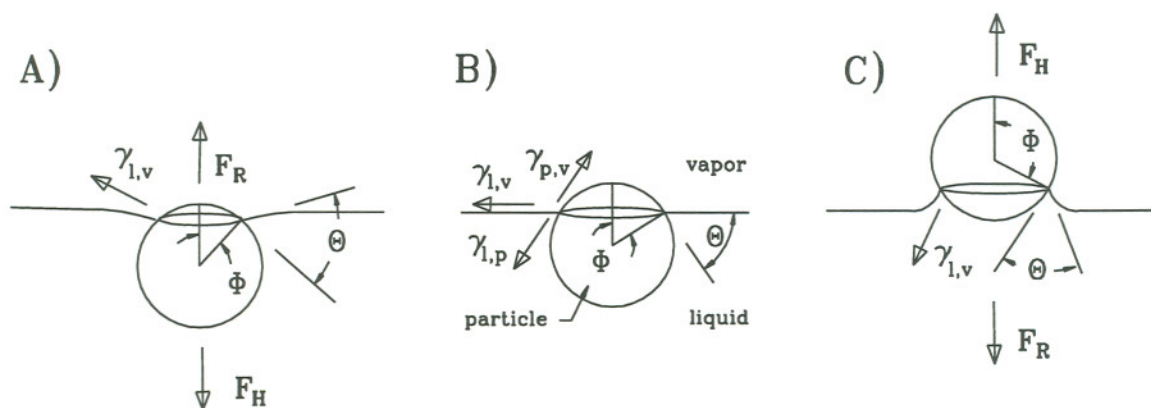


Figure 14. Components of the restoration force

- θ - fluid/particle contact angle
- ϕ - position of particle relative to triple-phase circle
- $\gamma_{l,v}$ - liquid/vapor surface tension
- $\gamma_{l,p}$ - liquid/particle surface tension
- $\gamma_{p,v}$ - particle/vapor surface tension
- F_H - hypothetical force displacing the particle
- F_R - restoration force attempting to push the particle back to equilibrium ϕ

Figure 15 depicts two instances of a vertical wafer emerging from a fluid bath. The wafer is rather hydrophilic, consequently a concave meniscus forms against the wafer. Near the wafer the slope of the meniscus is determined by the wafer contact angle (α). Only the meniscus region is shown, further out the fluid/vapor interface becomes horizontal. Stuck to the wafer is a hydrophilic particle. The wafer/particle adhesion force is represented by F_A .

As the wafer emerges from liquid to air the wafer meniscus will descend over the particle, ϕ will change from 0° to 180° , and the restoration force will act upon the particle. The restoration force has a component perpendicular to the wafer. This component is dubbed "extraction force" (F_E) when it is directed away from the wafer, and dubbed "compression force" (F_C) when it is directed toward the wafer.

As the wafer emerges from liquid to air, the particle will experience a growing extraction force (Figure 15 A) which will reach a maximum value, subside back to zero as ϕ passes through ϕ of equilibrium, then grow in the opposite direction (Figure 15 B), compressing the particle against the surface. The following equations are for the case of $0^\circ \leq \alpha \leq 90^\circ$; exchange "compression" and "extraction" for the case of $90^\circ \leq \alpha \leq 180^\circ$

$$\text{Maximum extraction force} \quad F_{E \max} = 2\pi R \gamma_{lv} \sin^2(\theta/2) \cos(\alpha)$$

$$\text{Maximum compression force} \quad F_{C \max} = 2\pi R \gamma_{lv} \sin^2(90^\circ + \theta/2) \cos(\alpha)$$

Leenaars reasons that if maximum extraction force exceeds adhesive forces then the particle will be extracted and carried away by the fluid interface. Restoration (thus extraction) force is proportional to the liquid surface tension ($\gamma_{l,v}$). Water has an unusually high surface tension, and therefore is a choice liquid in that respect. Extraction force is also dependent on a trigonometric relationship between ϕ and the solid/liquid contact angles of wafer (α) and particle (θ). F_E is maximized at 60° contact angles, provided $\theta = \alpha$. This is a reasonable restriction as wafer oxide and slurry particles are both composed of the same material - silica. Unfortunately, water has a very low contact angle on *un-modified* silica, yielding negligible extraction forces. However, chemical modification of the wafer and slurry facilitates the adjustment of these contact angles, producing a series of experimental samples with contact angles ranging from 5° to 90° . The high surface tension of water coupled with the 60° contact angle created optimal conditions for interfacial displacement to work.

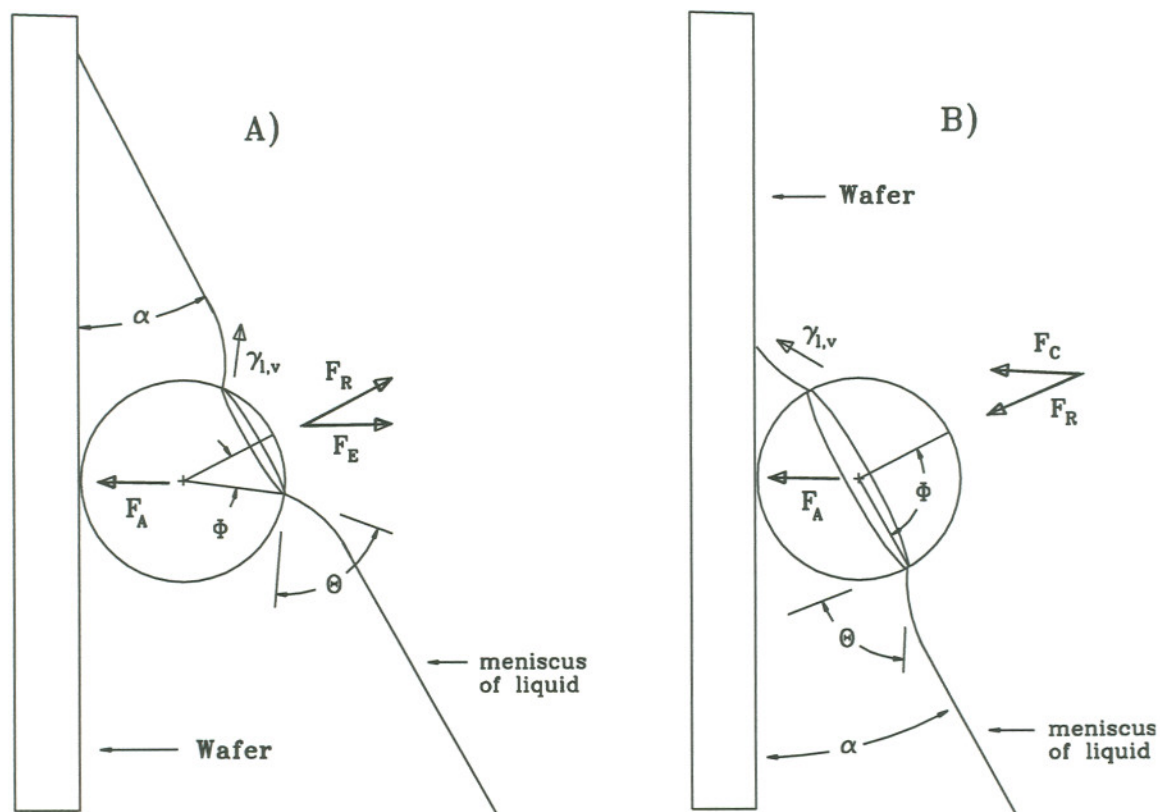
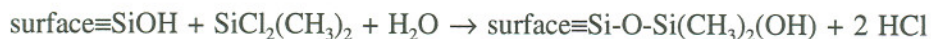


Figure 15. Components of extraction or compression forces

- α - fluid/wafer contact angle
- θ - fluid/particle contact angle
- ϕ - position of particle relative to the triple-phase circle
- $\gamma_{l,v}$ - liquid/vapor surface tension
- $\gamma_{l,p}$ - liquid/particle surface tension
- $\gamma_{p,v}$ - particle/vapor surface tension
- F_A - adhesive forces holding particle to wafer
- F_R - restoration force attempting to push the particle back to equilibrium ϕ
- F_E - extraction force, the component of F_R which is perpendicular to, and directed away from, the wafer
- F_C - compression force, the component of F_R which is perpendicular to, and directed toward, the wafer

Experimental results show that extraction of particles by passage through a fluid interface is ineffective for removal of dried-on slurry particles, despite extraction force optimization. This optimization of silica/water contact angles is the result of a chemical addition to the wafer and slurry surfaces - silanization from dichlorodimethylsilane ($\text{SiCl}_2(\text{CH}_3)_2$) which yields a silanized surface which is similar to that resulting from HMDS treatment.



This synthesis is impractical from a manufacturing standpoint, but was performed in this experiment to generate maximum possible extraction forces in order to demonstrate proof of concept. Water is desirable for its relatively large surface tension, but contact angle optimization is required to take advantage of the large surface tension. This optimization changes the silica/water contact angle from 5° to 60° and thereby increases the water interface extraction forces by a factor of nearly 20. Thus silanization facilitated use of both optimal surface tension and contact angle in this trial. Modeling showed substantially weaker extraction forces generated from simpler systems. These systems use liquids other than water and do not require surface modification to produce optimal contact angles.

Controlled silanization allowed the production of a series of samples of varying contact angles; those with values near 60° should be most susceptible to particle removal. None of the samples showed a reduction in particle counts (Table 4.) Both wafer emerging (rising from liquid) and wafer immersing (sinking into liquid) modes were both tested at 1.3 μm/sec. The modeled extraction force for water is about 57 mN/m for 60° contact angles. Van der Waals adhesive forces, for comparison, are about 27 mN/m for silica spheres on flat silica surfaces. If this model were applicable, and van Der Waals the only active adhesive force, then the particle should have been liberated.

The failure of this technique probably reflects the differing geometries between the model's ideal spherical particles and the actual nature of the silica particles. These particles are strings or flakes of smaller (perhaps spherical) pyrogenic beads. These aggregates may be broader than the interface boundary. Small spherical segments of the aggregate experiencing maximum extraction force at the interface are simultaneously anchored by the rest of the aggregate on either side of the interface, which is not experiencing any extraction force. Adhesive forces may also simply outweigh extraction forces, covalent attachment may well anchor the residual slurry to the wafer surface.

Conclusion: Extraction of particles by passage through a fluid interface is ineffective for removal of dried slurry despite optimization of silica/water contact angles.

Table 4. Extraction of Particles by Passage Through A Fluid Interface

<u>SiCl₂(CH₃)₂ Conc., μM</u>	<u>Contact Angles, degrees</u>				<u>Modeled Extraction Force/particle radius</u> mN/m	<u>Particle Counts</u>		
	<u>H₂O soak period</u>					<u>particles per 50x75 μm field</u>		
	<u>1 hr.</u>		<u>25 hr.</u>			<u>initial</u>	<u>pre- emersion</u>	<u>post- immersion</u>
	avg.	σ	avg.	σ				
0	10	2	3	0	2	~400	~400	~400
0	11	2	6	2	3	~400	~400	~400
0	13	4	4	1	3	~400	~400	~400
5	34	5	32	2	32	~400	~400	~400
13	42	3	51	1	47	~400	~400	~400
13	46	4	45	2	48	~400	~400	~400
32	55	3	52	2	55	~400	~400	~400
32	68	1	47	1	56	~400	~400	~400
80	66	3	69	2	53	~400	~400	~400
80	79	1	60	2	51	~400	~400	~400
200	89	1	76	1	27	~400	~400	~400
200	91	1	82	1	28	~400	~400	~400

4.3 Displacement of Wet Particles by Isopropanol

In this variation on the air/water theme described above, a 2-7 mm layer of liquid IPA condenses from IPA vapor and floats on the water surface, Figure 16. The resulting IPA-condensate/water interface is proposed to impart extraction forces on the adherent particles as wafers emerge through the interface.²⁶ The continuous condensation of IPA onto the emerging wafer surface is also reported to flush particulate-laden fluid away from the wafer surface. This sales literature fails to acknowledge that Leenaars' extraction mechanism requires taut interfaces and optimal contact angles. IPA and water are mutually miscible. Therefore the "surface tension" would be very low. The interface between IPA and water is very nebulous, as is its contact angle to silica. It is unreasonable to expect that this diffuse interface could impart any extraction force on particles.

Experimental results show that this system is ineffective at extracting DRIED slurry from wafers, but it is effective for preventing the deposition of WET slurry upon emersion from a slurry-contaminated rinse bath, Table 5. Silica slurry is instable in IPA. Upon introduction to IPA it coagulates and sinks. A likely mechanism for the observed deposition prevention is that the IPA displaces water from the wafer, along with any suspended particulate or dissolved contaminant contained therein. This then is a method which disrupts the entrainment mechanism (Figure 17).

The system appears to be sensitive to disturbances of the IPA/water interface. At high bath temperatures dripping condensate from the vessel's lid created waves which produced stratified particle deposits. The system is also dependent upon the presence of IPA vapor; wafers emerging through an IPA liquid layer without IPA vapor acquired a thick coating of aggregated silica particles.

Conclusion: Emersion of wet wafers through IPA was shown to reduce deposition of wet silica particle on emersion from a rinse bath by 90%. Removal of dried particles with the IPA/water interface was unsuccessful.

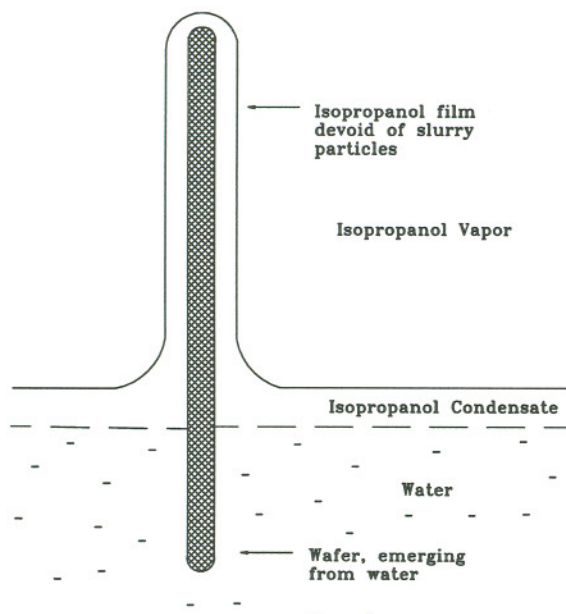


Figure 16. Displacement of wet particles by IPA. Entrainment of particles is inhibited. The IPA condensate displaces the particle laden water as the wafer emerges from the bath.

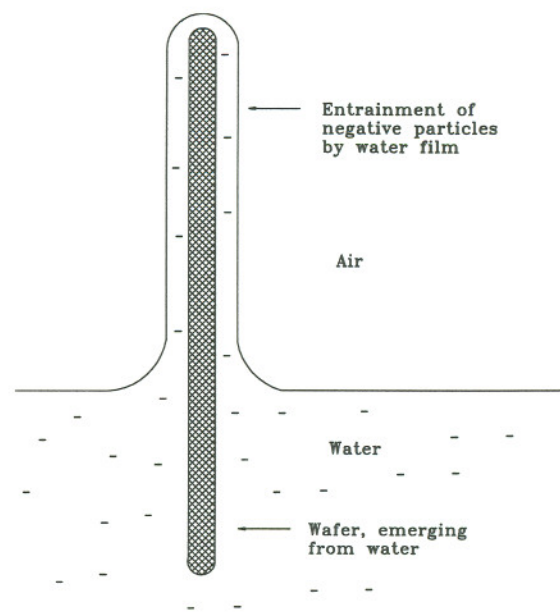


Figure 17. Entrainment of negatively charged particles. Suspended particles deposit onto a negatively charged hydrophilic wafer as the wetting water film evaporates after immersion.

Table 5. IPA Displacement of Wet Slurry, Data Summary

Emersion from 1/100 SS-25 bath at 0.01 cm/sec.

Group <u>Vapor/IPA Liquid</u>	Bath <u>Temp., °C</u>	# of <u>Trials</u>	# of <u>Wafers</u>	# of <u>Meas.</u>	Particles/Area*		Particle size/ <u>comments</u>
					<u>Avg.</u>	<u>Std.</u>	
Air/None (control)	18-20	2	9	54	49	28	1-2 μm aggregates
IPA Vapor/IPA Liquid	18-20	3	9	54	5	15	< 0.5 μm particles
IPA Vapor/IPA Liquid	72-80	2	9	54	289	444	stratified deposition
N ₂ or Air/IPA Liquid	18-20	3	12	72	1000's	N/A	> 20 μm floc

* particles per 50x75 μm microscope reticle @ 800x.

4.4 Adhesion Prevention via Chemical or Physical Bonding Inhibitors

The baseline post-polishing rinse process consists of aqueous rinsing of dilute slurry dispersions from polished wafers, followed by drying. It has been observed that any remaining dried residual particles are very difficult to remove from the wafers, in comparison to never-dried particles.

The first section reports on efforts to determine likely bonding mechanisms acting in the particle adhesion. These results show that bonding strengths can be reduced and rinsing improved as a result of the replacement of surface hydroxyls with alkyl groups, which are incapable of hydrogen bonding or silanol condensation. This silanization of slurry and wafer surface hydroxyls is aqueous-incompatible, thus not implementable as a processing improvement. The experimental motivation is purely diagnostic.

The second section reports on alternative caustic dispersion media. Potassium hydroxide is presently used to achieve high pH, but diffusion of alkali metals into semiconducting circuit elements is a potential contaminant. Alternative (non-metallic) bases were tested to observe their effects on slurry stability and adhesion.

The remaining sections report on the additions of agents to the post-polishing rinse water in attempts to replicate the silanization results via aqueous-born adsorbates introduced into rinse media. The objectives are 1) a reduction of the number of particles deposited during rinsing and drying; and 2) the reduction of post-drying adhesion strengths of any residual particles. The first objective is referred to as RINSING ENHANCEMENT, the second as REDUCED ADHESION. Both of these are evaluated relative to simple water rinsing of otherwise equal conditions (rinse water volume, slurry concentration, dynamics.)

The conditions of simplest implementation for any rinsing additive would be neutral to alkaline pH because concentrated pH 10.8 slurry dispersion is to be rinsed, eventually by neutral ultra-pure water. Acidification of the rinsing process would reduce double layer repulsion, perhaps sacrificing an advantage of the existing system. It would also add another critical variable to the process. Therefore, most adsorption experiments were carried out at high pH despite the fact that in many cases low pH would facilitate greater adsorption of cationic adsorbates. The primary motivation was to find an adsorbate that was effective at high pH.

In most cases the adsorbed agents provided new mechanisms for adhesion and induced slurry instability. Coagulation of the slurry yielded large aggregates and/or "water" (slurry) spots

which result in high post-rinsing particle counts. Sonication tests after drying suggest that some of these adsorbates reduce adhesion strength, however the initially high particle counts outweigh any advantages of reduced adhesion.

The notable exception to this trend is PEO. It is the most promising of the agents tested. It produced low particle counts both after the initial rinse (rinsing enhancement) and after sonication (adhesion reduction.)

The reader should take note of the qualitative nature of the "statistics" presented below, which are described on page 24. Most notable is that only large differences are significant, and that standard deviations associated with averages larger than 100 are artificially low.

Silanized Surfaces and Controlled Bonding Experiments

At least six mechanisms may contribute to the adhesion of slurry particles to the wafer surface: capillary adhesion, van der Waals attraction, hydrogen bonding, silanol condensation, hydrophilic bonding, and cationic bridging. These are described on page 12. Five of these require the presence of surface hydroxyl groups on one, if not both, opposing surfaces. It is possible to chemically transform the surface hydroxyls to alkylsiloxyl moieties, thereby eliminating many of the probable bonding mechanisms. A controlled bonding matrix was constructed in order to determine which mechanisms do contribute to the observed adhesion of the hydroxylated slurry. In the matrix the various combinations of hydroxylated or alkylsilanized slurry and wafer were tested for adhesion. The top (A) section of Table 6 shows which bonding mechanisms are possible in the various slurry-surface/wafer surface quadrants.

The degree of completion of the hydroxyl to silane transformation is somewhat controllable, thus a spectrum of four wafer-surface samples ranging from (assumed) completely hydroxylated (left column) to completely silanated (right column) was generated for the matrix. These modifications alter the hydrophobicity of the surfaces, so contact angle can be used to indicate relative degree of silanization.

The increased hydrophobicity also reduces the efficiency of particle deposition by the entrainment mechanism (page 14, 15.) These effects necessarily temper the evaluation of the controlled bonding data; rinsing effects attributable to inhibition of bonding mechanisms are not absolutely distinguishable from deposition reduction effects dependent on contact angle.

The dip coat experimental data (table 6-B) most clearly shows the importance of wettability for entrainment particle deposition. In this experiment four vertical wafers ranging from very hydrophilic to very hydrophobic were slowly emerged (0.01 cm/sec) from a bath of 1/100 SS-25 slurry dispersion. Only the most wettable (lowest contact angle) of the four retained a film and consequent particle deposition. These results suggests that:

- i) the entrainment model is valid (e.g. better rinsing can be achieved by increasing the wafers hydrophobicity);
- ii) *in situ* hydrophobization of wafers as part of the rinse process could reduce particle deposition (provided that the hydrophobization does not also facilitate NEW bonding mechanisms); and
- iii) in order to evaluate particle adhesion strengths on hydrophobic wafers, alternative dispensing medium will have to be employed in the experiment's particle deposition process. A nonaqueous dispersion media should be used to deposit slurry onto *hydrophobic* wafers. Isopropanol, or 50:50 volume IPA:water mixtures are therefore used in the matrix portion reported below. The catch-22 is that the (hydrophilic) SS-25 slurry is unstable in nonaqueous media, so dispersion media becomes an additional variable in the bonding experiments .

Spin coating was used to prepare samples for the bonding matrix; the data are presented in Table 6-C. Many possible particle/wafer bonding mechanisms possible in the upper left (hydroxyl surface) quadrant are impossible in the lower right (organosilyl surface) quadrant. Comparison between these two quadrants offer insight into which are the active bonding mechanisms.

Recall that emersion speed affects the entrainment particle deposition, and spin-coating is effectively a faster "emersion" than dip coating. Faster emersion result in higher particle counts. This could explain the successful spin-coating depositions on the moderately hydrophobic samples, where as the slower dip-coating was unsuccessful at depositing particles.

The results of the experiment are most obvious when comparing the upper left to lower right coordinates ($\equiv\text{SiOH}/\equiv\text{SiOH}$ and $\equiv\text{SiOSi}(\text{CH}_3)_2\text{OH}/\equiv\text{SiOSi}(\text{CH}_3)_3$ wafer/slurry combinations) of Table 6-C. In both combinations slurry deposition occurs. In the $\equiv\text{SiOH}/\equiv\text{SiOH}$ case

sonication fails to remove the dried residual slurry, whereas in the $\equiv\text{SiOSi}(\text{CH}_3)_2\text{OH}/\equiv\text{SiOSi}(\text{CH}_3)_3$ case the dried residual slurry is completely removed. Removal by sonication is also evident in the corners of the other diagonal - $\equiv\text{SiOSi}(\text{CH}_3)_2\text{OH}/\equiv\text{SiOH}$ and $\equiv\text{SiOH}/\equiv\text{SiOSi}(\text{CH}_3)_3$ wafer/slurry combinations. These results indicate that bonding mechanisms other than van der Waals and perhaps hydrogen bonding contribute to the strong adhesion of the (untreated) hydroxylated surfaces. These likely active mechanisms are: capillary adhesion, silanol condensation, and cationic bridging. This motivated further exploration of water compatible additives which would eliminate these bonding mechanisms which are dependent on the presence of silanol surface groups.

Alternative Caustic Media

This is somewhat of an orphan section, placed here more for fit-to-form than for function. Potassium hydroxide is presently used to achieve the high pH of the slurry dispersion, but diffusion of alkali metal contaminants into semiconducting circuit elements is a potential device liability. Alternative (non-metal) bases are being considered for device fabrication. These alternative caustic compounds are not particularly surface active, and are not expected to inhibit bonding. However, tests of these bases were requested to observe their effects on slurry stability and adhesion.

Aqueous solutions of **ethanolamine**, **cholinehydroxide**, and **tetramethylammonium hydroxide (TMAH)** show no improvement in rinsing; ethanolamine and TMAH destabilize the slurry resulting in flocculation and higher pre-sonication (post-rinsing) particle counts (Table 7.) All show some degree of adhesion reduction (low post-sonication counts, especially 200 mM TMAH. Ethanolamine may hydrogen bond to surface silanols, solvated cations of choline hydroxide and TMAH may bind as counter ions to deprotonated silica hydroxyls, thereby reducing adhesion strength by blocking silica-silica bonding.

Table 7. Alternative Caustic Media, Slurry-Particle Count/Area.Particle Counts per 50x75 μm microscope reticle @ 800x.

Separate Slurry and Wafer Treatments, 3 minutes.

monomer conc. :		<u>0 μM</u>		<u>1 μM</u>		<u>10 μM</u>		<u>100 μM</u>		<u>1000 μM</u>	
sonication status :		<u>pre</u>	<u>post</u>	<u>pre</u>	<u>post</u>	<u>pre</u>	<u>post</u>	<u>pre</u>	<u>post</u>	<u>pre</u>	<u>post</u>
ethanolamine pH 10 - 12	avg:	400	400	400	400	400	400	700*	288		
	std:	0	0	0	0	0	0	300	161		
	n:	12	12	12	12	12	12	6	6		
choline- hydroxide pH 10 - 14	avg:	400	400	400	400	400	135	400*	171		
	std:	0	0	0	0	0	163	0	194		
	n:	12	12	12	12	12	12	12	12		
		<u>0 mM</u>		<u>0.2 mM</u>		<u>2 mM</u>		<u>20 mM</u>		<u>200 mM</u>	
TMAH pH 10 - 13	avg:	400	400	400	400	400	400	700*	133	700*	33
	std:	0	0	0	0	0	0	300	189	300	75
	n:	12	12	12	12	12	12	6	6	6	6

* glaze coating of agent

Reagent Information

<u>Reagent</u>	<u>Structure</u>	<u>purity</u>	<u>Supplier</u>
ethanolamine	$\text{H}_2\text{NCH}_2\text{CH}_2\text{OH}$	99+%	Aldrich
choline hydroxide	$[\text{HOCH}_2\text{CH}_2\text{N}(\text{CH}_3)_3]^+\text{OH}^-$	-	Aldrich
TMAH	$[\text{N}(\text{CH}_3)_4]^+\text{OH}^-$	-	Moses Lake Industries

Surfactant Adsorption

The following sections report variations on a theme - the adsorption of a water soluble, surface active agent onto the slurry and wafer surfaces in order to create a barrier to intimate contact between the two silica surfaces and/or inhibit hydrogen bonding or silanol condensation between particle and wafer surfaces. Ideally this would improve rinsing and/or reduce adhesion. The variations are:

- 1) the identities of the agents; and
- 2) the consequent adsorption and adhesion-reduction mechanisms.

Hydrogen-Bond Inhibiting Solutes

Urea and **Guanidine HCL** are commonly used in biochemistry as strong hydrogen bonding agents to disrupt hydrogen bonding in protein structures. The amine hydrogens of these two molecules are hydrogen bond donors (of partial positive charge). Urea's amine nitrogen and carbonyl oxygen are hydrogen bond acceptors. Guanidine hydrochloride's amino nitrogen and imine nitrogen are hydrogen bond acceptors.

Glycerol is also capable of hydrogen bonding. Like silica, its hydroxyl oxygen is an acceptor and its hydroxyl hydrogen is a donor. **Micro Lab Soap®** is a commercial mixture of detergents and surfactants. It was thought that these agents might hydrogen bond to silica surface hydroxyls, thereby inhibiting hydrogen-bond adhesion or silanol condensation between silica particle and wafer surfaces.

Our experimental data (Table 8) show no rinsing improvements, and no adhesion reduction except for the possible reduction by 10 μM guanidine HCL. This is not repeated by the 100 μM sample, so its significance is diminished.

Table 8. Hydrogen Bonding Agents, Slurry-Particle Count/Area.

Particles per 50x75 μm microscope reticle @ 800x.											
Separate Slurry and Wafer Treatments, 3 minutes.											
monomer conc. :		<u>0 μM</u>		<u>1 μM</u>		<u>10 μM</u>		<u>100 μM</u>		<u>1000 μM</u>	
sonication status :		<u>pre</u>	<u>post</u>	<u>pre</u>	<u>post</u>	<u>pre</u>	<u>post</u>	<u>pre</u>	<u>post</u>	<u>pre</u>	<u>post</u>
urea pH 10	avg:	400	400	400	400	400	400	400*	400		
	std:	0	0	0	0	0	0	0	0		
	n:	12	12	12	12	12	12	6	6		
guanidine HCl pH 10	avg:	400	400	400	400	400	208	400*	400		
	std:	0	0	0	0	0	193	0	0		
	n:	12	12	12	12	12	12	12	12		
glycerol pH 10	avg:	400	400	400	400	400	373	400*	400		
	std:	0	0	0	0	0	88	0	0		
	n:	12	12	12	12	12	12	6	6		
		<u>0 %v</u>		<u>0.001 %v</u>		<u>0.01 %v</u>		<u>0.1 %v</u>		<u>1.0 %v</u>	
		<u>pre</u>	<u>post</u>	<u>pre</u>	<u>post</u>	<u>pre</u>	<u>post</u>	<u>pre</u>	<u>post</u>	<u>pre</u>	<u>post</u>
Micro lab soap pH 10	avg:	400	400	400	400	400	400	400	400	500*	400
	std:	0	0	0	0	0	0	0	0	224	0
	n:	12	12	12	12	12	12	6	6	6	6

* glaze coating of agent

Reagent Information			
<u>Reagent</u>	<u>Structure</u>	<u>purity</u>	<u>Supplier</u>
urea	H_2NCONH_2	99+%	Sigma Chemical
guanidine HCl	$[\text{H}_2\text{NC(=NH)NH}_2] \cdot \text{HCl}$	Reagent	Bethesda Research Lab
glycerol	$\text{HOCH}_2\text{CH(OH)CH}_2\text{OH}$	99+%	Aldrich
Micro Lab soap	mixture of detergents & surfactants	-	Baxter Scientific

Cationic Surfactant CTAB

Cetyltrimethylammonium bromide, $[\text{CH}_3(\text{CH}_2)_{15}\text{N}(\text{CH}_3)_3]^+\text{Br}^-$ or CTAB, is a common cationic surfactant. Monolayer adsorption of CTAB renders silica hydrophobic; bilayer adsorption results in charge reversal. The objective of this experiment was to adsorb a monolayer onto slurry and wafer surfaces in hopes of inhibiting the stronger silica-silica particle/wafer bonding mechanisms (hydrogen bonding and silanol condensation.) While CTAB adsorption may inhibit some of these mechanisms, it also introduces two new ones: hydrophobic attraction and cationic bridging.

The following characterization of adsorbed CTAB on mica surfaces is reported by Israelachvili.²⁷ Adsorption onto silica is thought to be similar given the two have surface siloxy groups and negatively charged surfaces. The two materials display very similar CTAB concentration dependencies on hydrophilicity/hydrophobicity transitions.²⁸ At concentrations much to slightly below the CTAB critical micelle concentration (CMC, $\sim 1000 \mu\text{M}$) a submonolayer to monolayer of the cationic quaternary ammonium cation adsorbs to a mica surface via bonding of its cationic head group to the deprotonated surface hydroxyls. This strong ionic bonding is augmented by the weaker van der Waals and intermolecular hydrophobic bonding. The hydrophobic tails extend away from the surface. This monolayer is reported to be 0.6 nm (submonolayer) to 1.8 nm (complete monolayer) thick. At higher concentrations a second layer forms tail-to-tail with the first so the second's head extends toward the solution. This results in charge reversal of the mica surface. The maximum double layer thickness is reported to be ~ 3.3 nm. Israelachvili²⁷ shows that under CTAB monolayer conditions on mica, surface attractive forces are present exceeding in strength and dissimilar in decay to van der Waals forces. This additional attractive force is attributed to be a hydrophobic (attractive) interaction between the CTAB alkyl groups on opposing surfaces.

Experimental data (Table 9) and observations show: 1), that slurry suspension remains (quasi) stable but that deposited aggregates increase in size (yielding high count averages and standard deviations) for the two samples below the CMC (10 and 100 μM) where submonolayer formation is expected; and 2), that rapid flocculation occurs at the approximate CMC. This suggests that at least one of three new mechanisms (hydrophobic interaction, cationic bridging, or collapse of the double layer) comes into play resulting in slurry instability. Once dried,

sonication does remove many of the aggregates indicating that bond strength has been reduced, presumably by the inhibition of either hydrogen bonding or silanol condensation.

This experiment shows that CTAB adsorption can reduce particle/wafer bond strengths, but that it also adversely affects the suspension stability. The deposition of larger aggregates is an undesirable result, so CTAB is an unlikely candidate for practical application to particle prevention.

Table 9. Monomer Surface-Active Agents, Slurry-Particle Count/Area.

Particles per 50x75 μm microscope reticle @ 800x.

Separate 1/100 SS-25 Slurry and Wafer Treatments, 3 minutes.

CTAB conc. :		<u>0 μM</u>		<u>1 μM</u>		<u>10 μM</u>		<u>100 μM</u>		<u>1000 μM</u>	
sonication status :		<u>pre</u>	<u>post</u>	<u>pre</u>	<u>post</u>	<u>pre</u>	<u>post</u>	<u>pre</u>	<u>post</u>	<u>pre</u>	<u>post</u>
CTAB	avg:	400	400	400	400	392	267	630	313	unstable,	
pH 10	std:	0	0	0	0	363	300	449	392	rapid floc	
	n:	12	12	18	18	18	18	12	18		

* glaze coating of agent

Polymer Surface-Active Agents

The effects of adsorption of three water soluble polymers (PVA, PEI, and PEO) and one block copolymer (PEO-PPO-PEO) are discussed in this section. General information about the polymers tested is listed in Table 10. It was thought that polymer adsorption would hinder silica-silica bonding mechanisms. Of the four, PEO shows the most promising results. Following separate or combined polymer adsorption treatment (page 22) of 1/100 SS-25 slurry and wafer, these modified dispersions were spin-coated (page 23) onto the wafers in order to mimic emersion from a rinse bath.

Typically three concentrations of each polymer were tested - 10, 100, and 1000 mg/l. The monomer units of the three polymer have molecular weights of either 43 or 44 g/mole, so the equivalent "molarities" of the three concentrations are 0.23, 2.3, and 23 "mM," respectively. For comparison, the surface hydroxyl concentration of 1/100 SS-25 is about 0.7 to 1.2 mM . In all cases spin-coating of the 1000 mg/l samples produced thin-films of cast polymer visible to the unaided eye.

Microscopic inspection shows these films to be thicker than slurry particles were tall; so the experimental distinction is lost between the effects of adsorbed polymer "mono" layers on adherent particles and thicker coated polymer films containing particles. 100 and 10 mg/l samples are believed to produce results attributable to adsorption alone; they often produced results distinctly different from (polymer-less) control samples yet had no discernible (optical microscope) thick polymer film (as did the 1000 mg/l samples.)

It is interesting to note that the 10 mg/l samples were effective at inducing aggregation even though the monomer unit to surface hydroxyl ratio was at most only about 1:3, and that the adsorption site to surface hydroxyl ratio was surely much less. Most polymers used had chain lengths on the order of 50 to 250 monomer units. Only a fraction of a chain's monomer units are involved in adsorption. (See "trains, loops, and tails" in the PEO section below.)

Table 10. General Information About Polymers Tested.

<u>Name</u>	<u>Abbr.</u>	<u>Structure</u>	<u>n</u>	<u>Polymer Avg. MW</u>	<u>Monomer MW</u>	<u>Source</u>	<u>Purity</u>
poly(vinylalcohol)	PVA	$-\text{[CH}_2\text{-CH(OH)]}_n\text{-}$	700 - 1100	31,000 - 50,000	44	Aldrich	87-89% hydrolyzed
poly(ethyleneimine)	PEI	$-\text{[CH}_2\text{-CH}_2\text{NH]}_n\text{-}$	42	1760	43	Polysciences	N/A
poly(ethyleneoxide)*	PEO	$\text{HO-[CH}_2\text{-CH}_2\text{-O]}_n\text{-H}$	14	600	44	Aldrich	N/A
"	"	"	72	1,000	"	Aldrich	N/A
"	"	"	45	2,000	"	Aldrich	N/A
"	"	"	110	4,600	"	Aldrich	N/A
"	"	"	140	6,000	"	J.T. Baker	N/A
"	"	"	230	10,000	"	Aldrich	N/A
"	"	"	450	20,000	"	Sigma	N/A
"	"	"	2300	100,000	"	Aldrich	N/A
"	"	"	14000	600,000	"	Aldrich	N/A

* AKA poly(ethyleneglycol)

PEO-PPO-PEO Block Co-Polymer Information

Trade Name: Pluronic® Surfactant (BASF Co.)

Chemical name: poly(ethyleneoxide)-poly(propyleneoxide)-poly(ethyleneoxide) block co-polymer

Structure: $\text{HO-[CH}_2\text{-CH}_2\text{-O]}_x\text{-[CH}_2\text{-CH}_2\text{-CH}_2\text{-O]}_y\text{-[CH}_2\text{-CH}_2\text{-O]}_z\text{-H}$

<u>Pluronic® Name</u>	<u>Avg. MW</u>			<u>Segment length, monomer units</u>		<u>Source</u>	<u>Purity</u>
	<u>Total MW</u>	<u>PEO MW, ea.</u>	<u>PPO MW</u>	<u>PEO, x,z</u>	<u>PPO, y</u>		
L43	1900	300	1300	6	22	BASF	N/A
L92	3700	400	2900	8	50	BASF	N/A
L122	5000	500	4000	11	69	BASF	N/A
L64	2900	600	1700	13	30	BASF	N/A
P103	5000	700	3500	17	60	BASF	N/A
F68	8400	3400	1700	76	29	BASF	N/A

Nonionic Polymer PVA

Polyvinyl alcohol (PVA) is a water soluble polymer. It is appealing in this study for its nonionic property, rendering it somewhat immune to double layer interactions. It can adsorb to silica by a variety of hydrogen bonding permutations. Hydrogen of either PVA's or silica's hydroxyls can serve as positive charge "donors"; the oxygens of either's surface can act as positive charge "acceptors". Silica surface siloxane can also be an acceptor. (Adsorption is maximized at an optimum siloxane:hydroxyl ratio, which reflects the degree of dehydration. This variable is not addressable in the scope of this study.) Adsorption is also maximized at the silica point of zero charge (pzc=pH 2) and decreases with increasing pH as deprotonation of surface hydroxyls reduces hydrogen bonding opportunities.²⁹ Increased adsorption of hydrated counter ions (sodium in this citation) may also block the PVA adsorption. This polymer is reported to cause flocculation of silica slurry at low PVA concentrations due to inter-particle bridging. Restabilization is achieved at higher concentrations once surface saturation is attained.

As stated above (page 40), adjustment of rinse conditions to low pH is undesirable from an implementation point of view. Therefore PVA (and other) experiments were performed at pH 10 despite the mechanistic preference for adsorption at low pH conditions.

The results of the PVA adsorption experiments are presented in the top row of Table 11. Some aggregation of slurry is observed at 10, 100, and 1000 mg/l PVA concentrations. Subsequent sonication does not remove the dried slurry suggesting that silica-silica adhesion mechanisms are either not hindered, or are replaced or augmented by polymer bridging.

The conclusion from this section is that PVA does not enhance rinsing or reduce adhesion strength, at least at pH 10. The adsorption restrictions of high pH may be significant; the results of low pH trials (where adsorption is favored) could be much different but are not pursued.

Synergistic Nonionic Polymer and Cationic Monomer, PVA & CTAB

A mechanism which is favorable at high pH for the adsorption of PVA to silica utilizes a molecular anchor of CTAB between the silica surface and the PVA polymer: "in the presence of preadsorbed CTA⁺ ions at high pH, the PVA adsorption increased significantly relative to the value in absence of surfactant."³⁰ The data of this citation at pH 10 shows a quadrupling of adsorption of 42,000 average MW PVA due to preconditioning by 20 μ M CTAB; PVA concentration ranges from 20 to 80 mg/l. Hydrophobic interaction between the hydrophobic

tail-up CTA⁺ monolayer and the ethyl segments of PVA is assumed to be responsible for this anchored bonding.

The results of the CTAB anchored PVA experiment are also presented in Table 11 in the second through fifth column. CTAB concentration seems to have more influence than PVA on aggregation. The high CTAB samples (fourth row) have the most aggregates, and addition of PVA does not improve the performance of the left (control) column. Some sonication-removal is apparent, especially at the 10 μ M CTAB, 100 mg/l PVA coordinants. This suggest that bond strengths are reduced and that bonding mechanisms may be inhibited. The magnitude of reduction is not impressive, nor are the statistics convincing. Significant rinsing enhancement and adhesion reduction by CTAB/PVA were not achieved.

Table 11. PVA with CTAB Anchor, Slurry-Particle Count/Area.

Particles per 50x75 μ m microscope reticle @ 800x.

Separate 1/100 SS-25 Slurry and Wafer Treatments, 3 minutes.

31,000-50,000 MW PVA:		0 mg/l		1 mg/l		10 mg/l		100 mg/l		1000 mg/l	
		<u>PVA</u>		<u>PVA</u>		<u>PVA</u>		<u>PVA</u>		<u>PVA</u>	
sonication status :		<u>pre</u>	<u>post</u>	<u>pre</u>	<u>post</u>	<u>pre</u>	<u>post</u>	<u>pre</u>	<u>post</u>	<u>pre</u>	<u>post</u>
0 μ M CTAB	avg:	400	400			379	361	500	383	500*	461
	std:	0	0			88	110	224	223	224	192
	n:	12	12			18	18	12	12	18	18
1 μ M CTAB	avg:	400	400			306	279	344	254		
	std:	0	0			162	152	331	281		
	n:	18	18			12	12	12	12		
10 μ M CTAB	avg:	392	267			347	223	273	124		
	std:	363	300			337	284	156	160		
	n:	18	18			12	12	12	12		
100 μ M CTAB	avg:	630	313			750	325	617	471		
	std:	449	392			296	254	331	396		
	n:	12	18			12	12	12	12		
1000 μ M CTAB	avg:	unstable,									
	std:	rapid floc									
	n:										

* thin film coating of polymer remains after particle deposition

Amphoteric Polymer PEI

Poly(ethyleneimine) (PEI) is a branched polymeric molecule with the structure $-(\text{CH}_2-\text{CH}_2-\text{NH})_x-$. Branches fork at occasional tertiary amines $\{\text{N}(-\text{CH}_2-)_3\}$. The amine becomes cationic with protonation $\{(-\text{N}^+\text{H}_2)-\}$. The degree of protonation decreases gradually with increasing pH; pH 10.8 is its point of zero charge.³¹ The degree of protonation affects both the size of the molecule (compact when uncharged) and adsorption mechanism. It can bond to silica by either of two mechanisms: by hydrogen bonding to silica surface hydroxyls when both are uncharged, or by coulombic attraction to anionic (deprotonated) surface hydroxyls when both are charged. Displacement of, or competition with, other cationic counter ions may inhibit the coulombic adsorption mechanism.

The two adsorption mechanisms present an interesting dilemma: cationic charge of the amine decreases with pH while anionic charge of the silica increases with pH. So the coulombic adsorption is maximized at some intermediate pH of compromise. Similarly, hydrogen bonding conditions each are optimal at opposite ends of the pH scale (2 for silica, 10.8 for PEI.) Thus adsorption and consequent stability or instability is highly sensitive to pH.³²

Molecular weight is important for its role in coverage and structure.³³ Slurry stability (and, by inference, particle adhesion) is dependent upon surface coverage of PEI on silica, upon the PEI structure, and the net charge of the particle. Flocculation results from the combined conditions of PEI extending out away from the surface, and sparse coverage of the surface by PEI. This enables inter-particle bridging of PEI (by either hydrogen bonding or coulombic.) Squat configuration and dense coverage coupled with charge reversal facilitates stabilization, or redispersion. As adsorption proceeds the system first enters a phase of instability (sparse coverage, bridging, neutrality); then, if concentration, pH, and molecular weight are right, enters a phase of restabilization (dense coverage, and charge reversal.)

Stability of the system is sensitive to pH, PEI molecular weight, and concentration. Redispersion is reported in some flocculation studies.³⁴ These results indicate that low molecular weight PEI (1760 MW) is most sensitive to pH (with neutral pH's being best) and that larger PEI (18,400) is relatively impartial to pH. This suggests that experimentation with larger PEI might prove fruitful.

The data (Table 12) show that rinsing with aqueous solutions of 1800 molecular weight PEI at pH 2, 6, and 10 causes flocculation, increasing the number of particles remaining after

rinsing. Many of these particles could be removed by sonication in IPA suggesting that adhesion strength is reduced relative to untreated slurry. Redispersion arises from charge reversal of the silica, resulting from adsorption of cationic PEI. It was thought that redispersion might improve rinsing and reduce adhesion. From a practical standpoint, however, the necessity of crossing an unstable phase region prior to establishment of redispersion renders this approach less promising than the nonionic polymers reported below.

Table 12. PEI Polymer Surface-Active Agents, Slurry-Particle Count/Area

Particles per 50x75 μm microscope reticle @ 800x.

Separate 1/100 SS-25 Slurry and Wafer Treatments, 3 minutes.



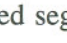

polymer conc. :	<u>0 mg/L</u>		<u>1 mg/L</u>		<u>10 mg/L</u>		<u>100 mg/L</u>		<u>1000 mg/L</u>		
	sonication status :		<u>pre</u>	<u>post</u>	<u>pre</u>	<u>post</u>	<u>pre</u>	<u>post</u>	<u>pre</u>	<u>post</u>	
PEI 1800 MW pH 2	avg:				761	679					
	std:				300	387					
	n:				18	19					
PEI 1800 MW pH 6	avg:				347	223					
	std:				337	284					
	n:				12	12					
PEI 1800 MW pH 10	avg:	445	459	400	325	843	476	654	476	598*	388
	std:	204	195	0	150	263	384	296	384	341	398
	n:	28	27	5	5	26	22	26	22	25	26

* thin film coating of polymer remains after particle deposition

Nonionic Polymer PEO

Poly(ethyleneoxide) (PEO, also called poly(ethyleneglycol) or PEG) was found to both enhance rinsing of wet slurry and reduce adhesion of dry PEO treated particles. These improvements show a dependence on PEO molecular weight. For combined-treatment trials the rinsing enhancement consists of about 90% fewer particles remaining for rinsing of wet slurry with 100 mg/L pH 10 aqueous solution of 10,000 MW molecular weight PEO.

PEO is a linear polymeric molecule with the structure $\text{HO}-(\text{CH}_2-\text{CH}_2-\text{O})_x-\text{H}$. Solubility and adsorption characteristics vary with molecular weight, which is dependent on chain length (x). Generally, it is infinitely water soluble, and soluble in many organic media. It adsorbs to silica surfaces via hydrogen bonding between its ether oxygen atoms and the surface hydroxyl groups.³⁵

When adsorbed to a surface, substantial portions of the long PEO molecule stand away from the surface,³⁶ somewhat like a "W" or a "" contacts the baseline (surface) in only a few places. The unattached segments are called tails () or loops () the attached segments are called trains () Loops and tails remain in continuous motion and hold a collection of water molecules about them. If two surfaces which are saturated (or nearly so) with such adsorbed PEO layers are forced together then water is expelled from the gap between the two surfaces and the loop and tail motion also becomes restricted. Together this expulsion and restriction act to resist further compression of the two surfaces^{37,38}; the resulting resistance to

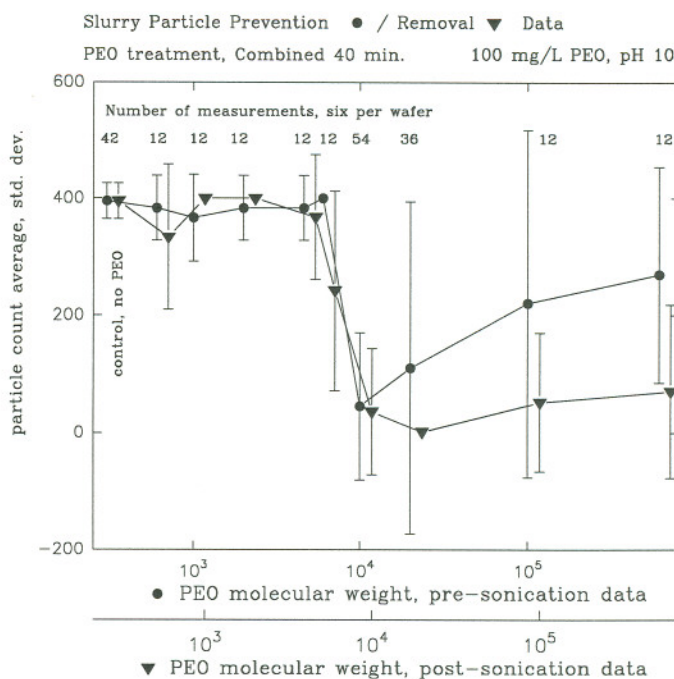


Figure 18. PEO molecular weight dependence for rinsing and adhesion strength in combined-treatment trials. PEO consistently shows enhancement of particle rinsing with 10,000 MW PEO and a reduction of adhesive strength of residual particles by 20,000 MW and larger PEO molecules. Enhanced rinsing is evident by low pre-sonication particle counts (circles); reduced adhesion is evident by post-sonication counts (triangles) decreased from pre-sonication counts. Increased aggregation contributes to larger standard deviations with increased molecular weight.

compression is called steric repulsion. When exploited to promote stability of a dispersion this phenomenon is called steric stabilization. If the surfaces *are not* nearly saturated and the tails or loops *are* long enough then the loop attached to one surface may bond to a bare spot on the opposite surface. This inter-particle bridging leads to dispersion instability and particle aggregation,³⁹ a condition which may also promote particle adhesion to wafer surfaces.

The success of steric stabilization depends on the sizes and relative distributions of trains, loops and tails,⁴⁰ which in turn vary with PEO molecular weight, PEO concentration, and solution pH and ionic strength.

In this work a dependence on molecular weight was found for PEO's rinsing improvement and adhesion reduction as shown in Figure 18 and Table 13. Both separate and combined-treatment trials were performed with molecular weights varying from 600 to 600,000 MW, which corresponds to chain length varying from 14 to 14,000 monomer units. In both cases it was found that 10,000 and 20,000 MW PEO were most effective for rinsing enhancement and adhesion reduction. Smaller molecular weights were not effective. Molecular weights larger than 20,000 were somewhat less effective than the 10,000 and 20,000 samples. Recall that loop and tail size is also dependent on molecular weight. Based on these observations the following hypothesis was developed to explain the rinsing improvement from 10,000 MW and 20,000 MW PEO. Attempts to confirm this hypothesis are reported on page 70.

- a) Loops and tails from small PEO (<10,000 MW) are too short for steric repulsion forces to significantly augment the existing electrostatic DLVO repulsion forces.
- b) Loops and tails from medium PEO (10,000 and 20,000 MW) are long enough (and surfaces saturated enough) for steric repulsion forces to significantly augment the existing DLVO repulsion forces.
- c) Surfaces unsaturated by large PEO (>20,000 MW) experience bridging or intersegmental attraction of long loops and trains reaching beyond the effective range of DLVO repulsion, leading to instability and aggregation.

An alternative explanation for the rinsing improvement results from the PEO induced increase in wafer hydrophobicity. This hinders wetting by the slurry dispersion, thereby inhibiting the entrainment mechanism for particle deposition. The particle-laden dispersion simply rolls off the wafer rather than wetting it and depositing particles via evaporation of the dispersion media. In other experiments using non-aqueous treatments, similar rinsing enhancement due to hydrophobization was observed from the silanizing agent dichlorodimethylsilane. This agent does not exhibit steric stabilization. Aqueous slurry would not deposit onto these very hydrophobic wafers.

Effects of pH are presented in Table 14; the observed behavior was consistent with steric stabilization theory and published reports.⁴¹ Flocculation increases with decreasing pH; thus high pH is desirable. These are the conditions of present processing; implementation of PEO rinsing would not require additional pH adjustment.

X-ray photoelectron spectroscopy (XPS) analysis shows that PEO can be removed from wafers by either of the common sulfuric acid/hydrogen peroxide (Piranha) or ammonium hydroxide/hydrogen peroxide (RCA SC-1) cleans, Figure 19. Simpler rinses in water or isopropanol were not effective for complete removal of PEO.

Table 13. PEO Polymer Surface-Active Agents, Slurry-Particle Count/AreaParticles per 50x75 μm microscope reticle @ 800x.

		Separate 1/100 SS-25 Slurry and Wafer Treatments, 3 minutes.						Combined 1/100 SS-25 Slurry and Wafer Treatments, 50 minutes.					
		<u>0 mg/L</u>		<u>100 mg/L</u>		<u>1000 mg/L</u>		<u>0 mg/L</u>		<u>100 mg/L</u>			
polymer conc. :	sonication status :	<u>pre</u>	<u>post</u>	<u>pre</u>	<u>post</u>	<u>pre</u>	<u>post</u>	<u>pre</u>	<u>post</u>	<u>pre</u>	<u>post</u>		
PEO 600 MW pH 10	avg:	396	378	400	400	400*	135	395	395	383	334		
	std:	27	72	0	0	0	188	30	30	55	124		
	n:	111	120	5	6	5	6	42	42	12	12		
PEO 1,000 MW pH 10	avg:	"	"	400	367	400*	177	"	"	367	400		
	std:	"	"	0	75	0	170	"	"	75	0		
	n:	"	"	5	6	5	6	"	"	12	12		
PEO 2,000 MW pH 10	avg:	"	"	300	367	400*	164	"	"	383	400		
	std:	"	"	126	75	0	182	"	"	55	0		
	n:	"	"	5	6	10	11	"	"	12	12		
PEO 4,600 MW pH 10	avg:	"	"	400	340	400*	242	"	"	383	368		
	std:	"	"	0	120	0	181	"	"	55	107		
	n:	"	"	5	5	10	11	"	"	12	12		
PEO 6,000 MW pH 10	avg:	"	"	280	225	400*	245	"	"	400	242		
	std:	"	"	98	176	0	188	"	"	0	170		
	n:	"	"	5	6	10	11	"	"	12	12		
PEO 10,000 MW pH 10	avg:	"	"	52	0	370*	17	"	"	45	36		
	std:	"	"	115	1	393	55	"	"	125	108		
	n:	"	"	30	30	11	12	"	"	54	53		
PEO 20,000 MW pH 10	avg:	"	"	32	1	347*	20	"	"	111	1		
	std:	"	"	102	3	109	55	"	"	283	5		
	n:	"	"	29	30	10	12	"	"	36	36		
PEO 100,000 W pH 10	avg:	"	"	400	317	460*	61	"	"	221	52		
	std:	"	"	0	121	180	118	"	"	297	118		
	n:	"	"	5	6	10	12	"	"	12	12		
PEO 600,000 MW pH 10	avg:	"	"	400	283	350*	112	"	"	270	71		
	std:	"	"	0	167	87	134	"	"	184	148		
	n:	"	"	5	6	4	6	"	"	12	12		

* thin film coating of polymer remains after particle deposition

Table 14. PEO and pH, Slurry-Particle Count/Area

 Particles per 50x75 μm microscope reticle @ 800x.

Separate 1/100 SS-25 Slurry and Wafer Treatments, 3 minutes.

sonication status:		pH 4		pH 7		pH 10	
		pre	post	pre	post	pre	post
PEO 0 MW (control)	avg:	400	233	400	400	400	400
	std:	0	170	0	0	0	0
	n:	6	6	6	6	6	6
PEO 2,000 MW	avg:	800	350	170	1	400	400
	std:	0	122	371	1	0	0
	n:	6	6	6	6	6	6
PEO 6,000 MW	avg:	733	634	1	0	68	1
	std:	149	335	1	1	149	1
	n:	6	6	6	6	6	6
PEO 10,000 MW	avg:	800	500	233	500	0	2
	std:	200	224	373	500	0	1
	n:	6	6	6	6	6	6
PEO 20,000 MW	avg:	967	567	567	202	167	216
	std:	75	453	453	364	373	357
	n:	6	6	6	6	6	6
PEO 100,000 MW	avg:	60	251	533	167	405	1
	std:	283	364	359	372	442	1
	n:	6	6	6	6	6	6

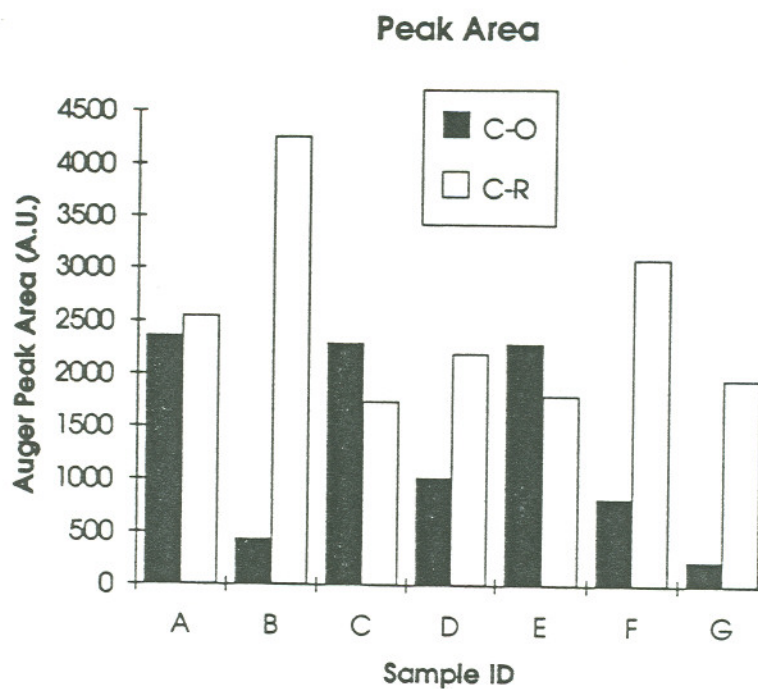


Figure 19. XPS data for various cleaning techniques. The black bars indicate XPS signal (287.0 eV) strength of the PEO C-O bonds. Cleaning processes F and G are the most effective for removal of PEO and are standard industrial cleaning solutions.

<u>Sample</u>	<u>Cleaning Process</u>
---------------	-------------------------

- | | |
|---|--|
| A | None. This represents full XPS signal strength for an un-cleaned PEO-coated surface. |
| B | None. This represents the background noise level of a wafer having never seen PEO. |
| C | Sonication in isopropanol. |
| D | Boiling water. |
| E | Sonication in water. |
| F | Boiling ammonium hydroxide and hydrogen peroxide solution (RCA SC-1.) |
| G | Boiling sulfuric acid and hydrogen peroxide solution (Piranha.) |

Nonionic Block Copolymer PEO-PPO-PEO

Poly(propyleneoxide) (PPO) can be combined covalently with PEO to form a surface-active block copolymer. Six commercially available copolymers (Pluronic®, BASF Co.) of the configuration PEO_x-PPO_y-PEO_z were used in these studies (Table 10.) PPO is less soluble in water than is PEO; variation of the values x and y is used to tailor the copolymer's solubility and adsorption characteristics.⁴²

Three concentrations of each copolymer were used in the preliminary separate-treatment experiments. The most promising of these (P103 at 100 mg/L) was then tested in larger separate-treatment trials, and finally compared to pure PEO results using combined-treatments. The results are similar to, but less impressive than those of the 10,000 and 20,000 MW PEO. Slight rinsing enhancement is observed from F68, L92, and P103 at 100 mg/L; all show moderate to good adhesion reduction as evidenced by sonication removal (Table 15.)

In light of the steric repulsion hypothesis, the poorer performance relative to pure PEO is probably attributable to the smaller sizes of the copolymer's PEO segments. Pure PEO performed best at molecular weights of 10,000 MW and 20,000 MW; the largest PEO segment of the copolymer sample was only 3,400 MW. (The largest available from BASF is F108 with 5,800 MW PEO segments.) Within the group tested at 1000 mg/L there is some correlation between adhesion reduction and PEO segment size. There are no correlations between rinsing enhancement or adhesion reduction and segment sizes at 100 mg/L.

Table 15. PEO-PPO-PEO, Slurry-Particle Count/Area

Particles per 50x75µm microscope reticle @ 800x						
Pluronic® Formula	Rinsing Enhancement (pre-sonication)			Adhesion (post-sonication)		
	avg.	std.	n	avg.	std.	n
<u>Separate Slurry and Wafer Treatments, 3 minutes</u>						
0 mg/L control	396	27	111	378	72	120
10 mg/L						
L43	400	0	10	297	169	11
L92	380	60	10	473	260	11
L122	380	60	10	218	150	12
L64	380	60	10	317	151	12
P103	400	0	10	122	169	12
F68	400	0	10	234	178	12
100 mg/L						
L43	400	0	5	333	94	6
L92	326	148	5	4	4	6
L122	400	0	5	300	141	6
L64	400	0	5	58	72	6
P103	290	205	29	55	119	30
F68	320	98	5	160	150	5
1000 mg/L						
L43	460	180	10	274	152	11
L92	400	0	10	252	283	12
L122	400	0	10	100	126	11
L64	400	0	10	128	146	11
P103	400	0	9	52	118	12
F68	584	357	10	92	148	12
<u>Combined Slurry and Wafer Treatment, 40 minutes</u>						
0 mg/L control	395	30	42	395	30	42
100 mg/L						
P103	389	46	18	256	186	18
10 k MW PEO	45	125	54	36	108	53
20 k MW PEO	111	283	36	1	5	36

CHAPTER 5

AFM MEASUREMENT OF ADHESIVE/REPULSIVE FORCES

Direct measurements of adhesive/repulsive forces and their dependence on pH and ionic strength are as expected - showing that high pH and low ionic strength are desirable. Measurements failed to display the suspected steric forces generated by adsorbed 10,000 MW PEO, but unexpectedly did show them for 6,000 MW PEO. These measurements illustrate some surface chemical principles using an uncommon but increasingly useful application of an emerging AFM technology.

An atomic force microscope (AFM) can be configured so as to measure the net intermolecular force generated between its stylus and a test surface as a function of separation distance between the two. The stylus, or "tip" is attached to a cantilever. The test surface is mounted to piezoelectric stage which allows control of horizontal and vertical positioning. The distance between test surface and stylus is gradually reduced (approaching) or increased (retracting) while the separation-distance dependent deflection of the stylus is measured as photodiode response to a laser beam reflected from the cantilever. This measured deflection is proportional to the force generated between surface and stylus. The force is calculated from the deflection using Hooke's law and the spring constant of the cantilever. The separation-distance between stylus and test surface is determined from piezo position and information derived from the linear "contact" region of the data, Figure 20.

These measurements can be made in a fluid environment. Thus interactions between "particles" (stylus tip) and test surfaces (wafer) can be measured in various solution conditions. A limited number of such measurements were made in an attempt to confirm the PEO hypothesis (page 58.) This opportunity also allowed the measurement of pH and ionic effects.

An artifact of the measurement mechanism is that force/distance gradients steeper than the cantilevers spring constant cannot be recorded. Upon reaching this threshold the stylus jumps abruptly from a finite separation distance into contact with the sample on approach, and jumps out of contact on retraction. Thus, "jump-in" and "jump-out" discontinuities occur in some

force/distance profiles. Resolution can be improved with stiffer cantilevers, but at the cost of sensitivity.

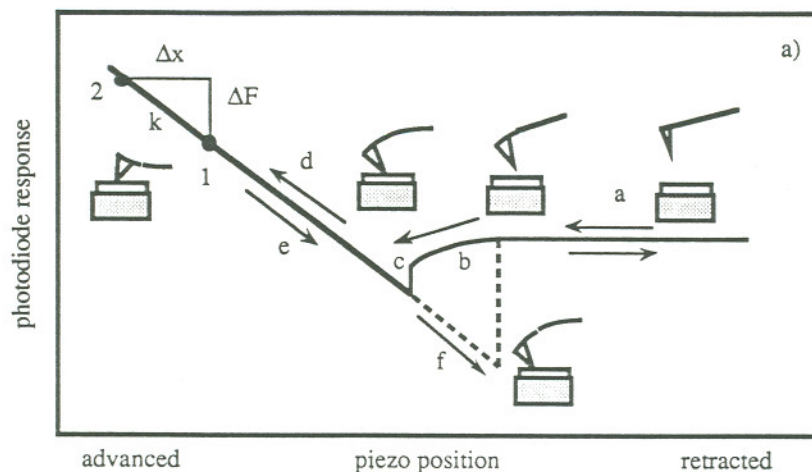


Figure 2a. A schematic of a typical AFM force-distance plot using unmodified tips. The arrows show how the force plot is generated as the sample is advanced and retracted. At (a) the tip and sample are far apart. When the tip gets close enough to experience the attractive van der Waals force, the cantilever starts to bend (b). When the force gradient exceeds the cantilever spring constant, the tip jumps into contact with the surface (c). Once in contact, the tip and sample move the same amount as shown by the linear portion (d). Upon the retraction (e), the cantilever relaxes a distance equal to the amount the sample has been retracted. If there is an adhesive force, then there is hysteresis in the loop (f). The inset depicts the state of cantilever bending. Positions 1 and 2 show how to calibrate the force scale. The distance the cantilever has moved, Δx , multiplied by the spring constant, k , yields the force difference, ΔF , between the two positions.

Figure 20. Schematic and explanation of AFM measurement apparatus, from reference 47. This "force-distance plot" is more precisely a cantilever-deflection(photodiode response)/piezo-(sample's vertical) position plot. After initial collection, these typical data are transformed algebraically to the force/distance profiles as presented on the following pages.

Ideally, the stylus tip would be a spherical silica particle attached to a commercial AFM cantilever - silica in order to measure the effects characteristic of that material, spherical in order to normalize the data. The forces generated are modeled to be directly proportional to the radii of spherical probes, the force data are often presented as force/probe radius. Other investigators⁴³ have successfully assembled and used such tips, and this too was our plan. Unfortunately, we were unable to produce usable spherical silica tips within the limited AFM time allotment. As a contingency then, measurements were made using the commercial pyramidal silicon nitride AFM tip. The slightly blunt tip as the serving as the test "particle," and a regular test wafer serving as

the silica surface. Fortunately, at high pH the silicon nitride tip behaves like silica,⁴⁴ (its surface supporting both Si-OH and some Si-NH₂) and so is assumed to be a reasonable substitute for a silica (slurry) particle. Equipment and stylus information are given on page 26 ("Direct Force Measurements...")

Spherical tip geometry is desirable for convenient normalization and comparison to theoretical models. Following convention, we have normalized force values by the apparent "radius" (40, 50 or 80 nm) of the somewhat rounded blunt top of the 3600 nm tall pyramidal stylus. The resulting force/radius values are about 50 times greater than those of theoretical expectation and published studies using spherical (AFM)⁴³ or cylindrical (surface force apparatus)⁴⁵ silica probes. Our corresponding un-normalized force values (not graphed) do agree well with those of published reports utilizing similar Si₃N₄ AFM tips and solution conditions⁴⁶ (variable pH.) Despite the dubious absolute force/radius values, the data collected can be used to illustrate relative effects of the various solution conditions.

Influence of pH and Ionic Strength

DLVO theory predicts that like-charged (ionic double layer) surfaces approaching one another will, at long ranges, experience growing mutual repulsion until sufficiently close (a few nanometers) that the short range van der Waals attraction dominates and the surfaces will then be attracted to one another. Conversely, oppositely charged surfaces will be increasingly attracted to one another from long distances. An increase in ionic strength will decrease the strength of the double layer repulsion or attraction.

Silica is increasingly negatively charged above pH 2. Silicon nitride is negatively charged above pH 6.8, and positively charged below pH 6.8. Thus the double layer interaction between the Si₃N₄ tip and silica surface will be repulsive below pH 2, attractive between pH 2 and 6.8, and again repulsive above pH 6.8.

The measured influence of pH and ionic strength (KCl electrolyte concentration) is displayed in Figure 21. The pH of the samples labeled "~7" were assumed from solution composition ("pure" deionized water), but not actually measured nor buffered. (At the time of the data collection, pH 7 behavior was not of interest, nor was silicon nitride's pH 6.8 isoelectric point recognized.) It is conceivable that adsorption of atmospheric CO₂ reduced the pH below 6.8, which would account for the long-range attraction of the "pH ~7" samples. Charge reversal of

the tip (positive to negative) with increase of pH to 10 (measured) results in mutual repulsion. In either pH case addition of electrolyte (KCl) reduces the strength of the double layer and the magnitude of attraction or repulsion. The observed effects of pH and ionic strength are consistent with DLVO theory, supporting rinsing with high pH and low ionic strength solutions in order to maximize double layer repulsion.

Jump-in and jump-out occurs at low ionic strength with tip #1 but not #2. This suggests that tip #2 and/or the complementary surface sample may be contaminated, inhibiting intimate contact and establishment of van der Waals attraction between the tip and silica surface.

Retraction of tip #1 (Figure 22) shows the relative strengths of the net short-range attractive forces responsible for the jump-out. Attraction is reduced by increasing pH because of charge reversal of the Si_3N_4 double layer. At low pH (hollow circles) both of the DLVO components are attractive, at high pH (hollow diamonds) the double layer contribution becomes repulsive while the van der Waals remains attractive, reducing the net attraction.

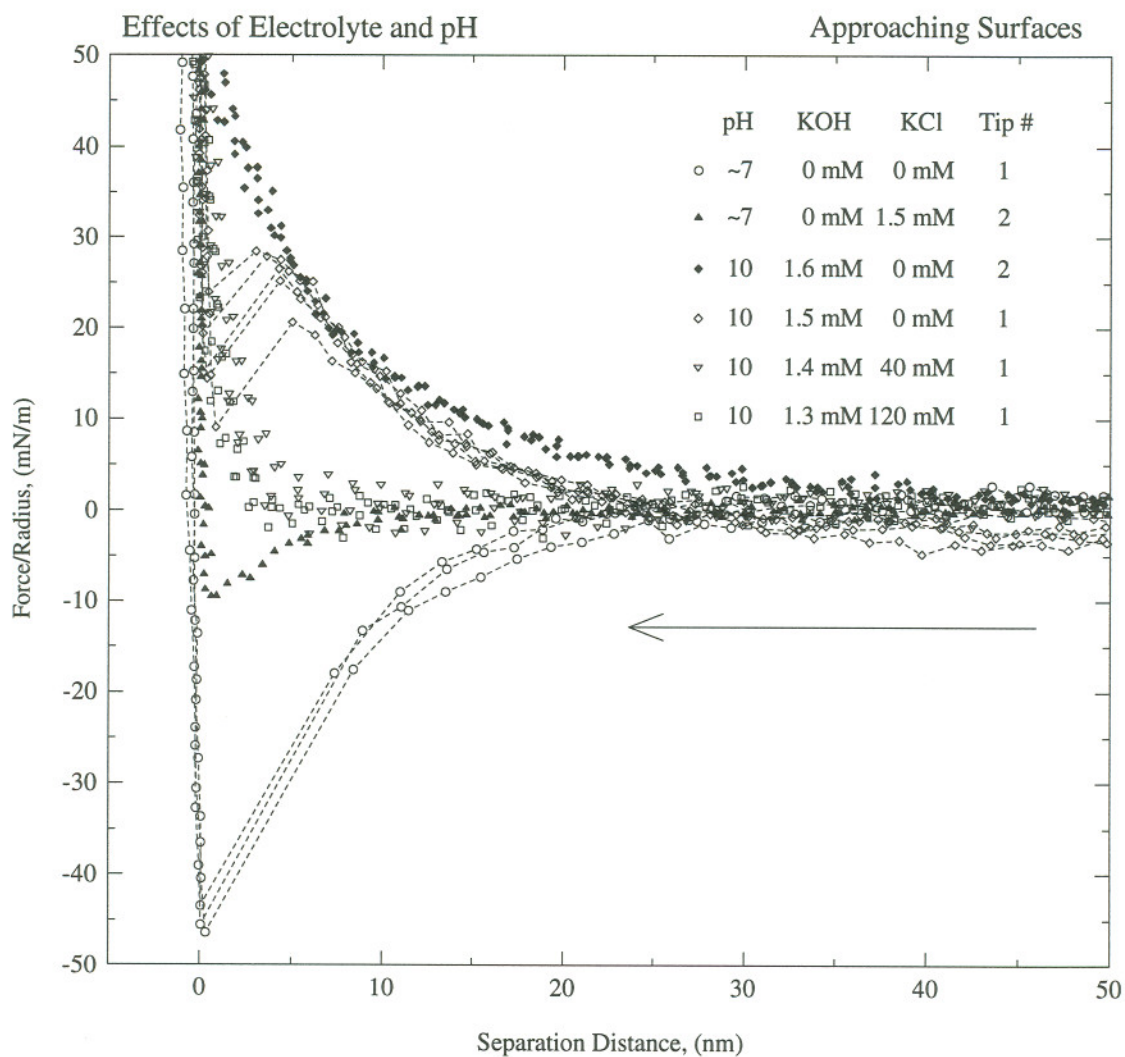


Figure 21. AFM Force-Distance Profiles: approaching surfaces, Si_3N_4 tip #1 (hollow figures) and #2 (solid) data, and HF etched SiO_2 wafer. Magnitudes of attraction and repulsion decrease as ionic strengths increase. Attraction shifts to repulsion as pH changes from <6.8 (est.) to 10 due to charge reversal (positive to negative) of Si_3N_4 , silica remains negative over this range. Jump-in is observed at low ionic strength for tip #1 (hollow circle and hollow diamond), but not for tip #2. This implies that tip #2 and/or the complementary surface sample bore a contamination layer which screened the van der Waals attraction.

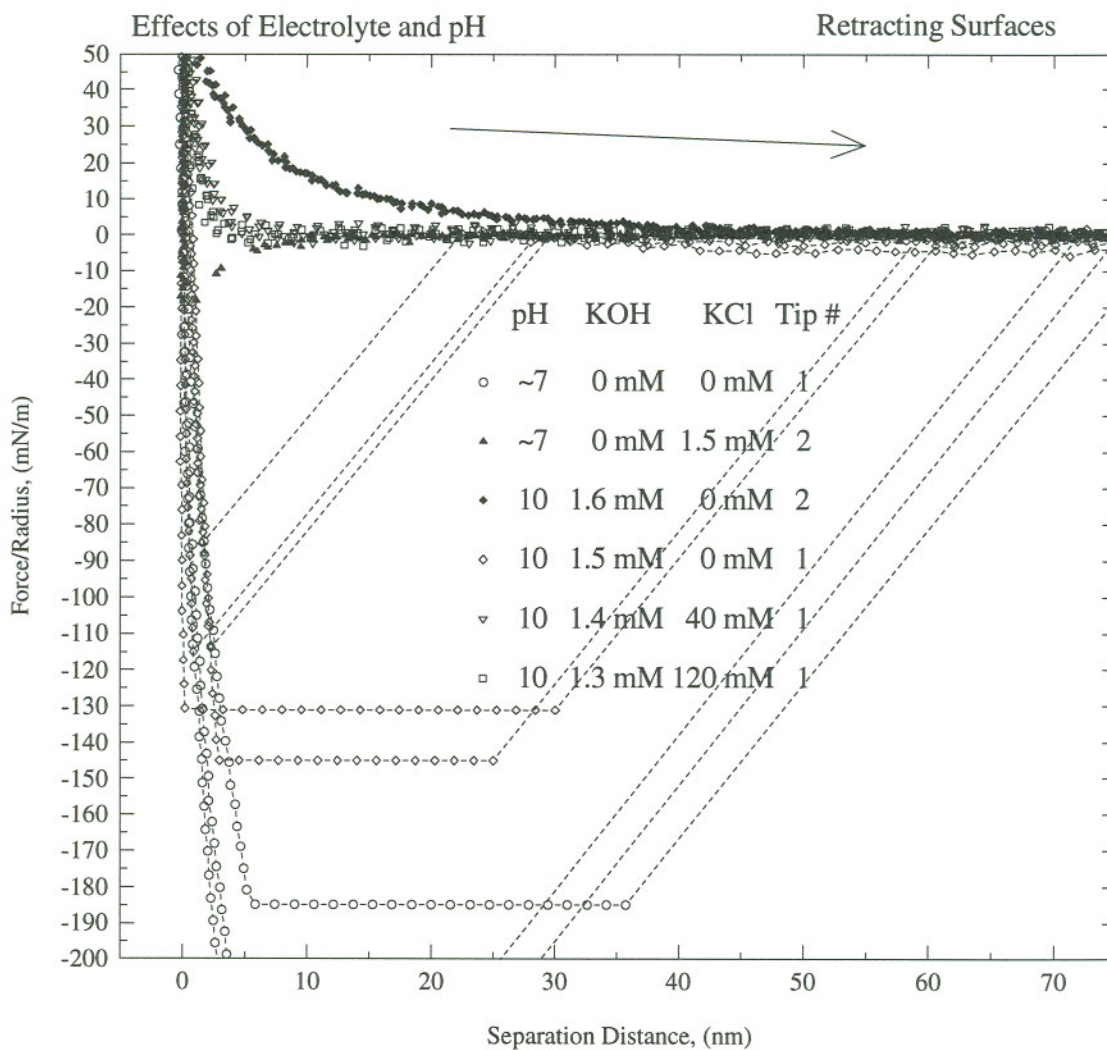


Figure 22. AFM Force-Distance Profiles: retracting surfaces, Si_3N_4 tip #1 (hollow figures) and #2 (solid data), and HF etched SiO_2 wafer. Note scale change. Tip #1's jump-out on retraction indicates strong short-range attraction. Attraction is greatest for pH ~7 (assumed <6.8) due to combination of van der Waals and double layer attraction (hollow circles). The double-layer interaction component becomes repulsive at pH 10 while the van der Waals component remains attractive, thus net attraction is reduced (hollow diamonds). Drastic contrast is seen for tip #2 in identical conditions (solid diamonds). A possible contamination layer would prevent intimate contact and inhibit establishment of van der Waals attraction. The horizontal sections are spurious products of signal processing: cantilever deflection extending beyond maximum detectable limits.

Influence of Adsorbed PEO

Steric repulsion is believed to be responsible for the PEO rinsing enhancement and its molecular weight (MW) dependence. By this hypothesis, adsorption of 10,000 MW PEO would produce steric repulsion which would substantially add to the double layer electrostatic repulsion, while the smaller 6,000 MW PEO would not (page 58.) Atomic force measurements (AFM) do show the expected reduction of electrostatic repulsion by increasing electrolyte but, contrary to the hypothesis, do not indicate additional repulsion due to adsorption of 10,000 MW PEO, Figures 23 and 24. AFM does show additional repulsion from 6,000 MW PEO, again contrary to our hypothesis, Figure 25 and 27.

The hypothesis is still believed to be valid, however. Measured steric effects of PEO are widely reported using AFM⁴⁷ and crossed cylinder⁴⁸ techniques. The unexpected result most likely reflects the experiment's limited sample size and unrefined technique. Steric repulsion is dependent upon surface saturation by PEO, which may not have been achieved in the 10,000 MW sample. Other investigators^{47, 48, 49} allow several hours for saturation and have shown increasing repulsion as adsorption develops over time to saturation. This study's measurements were limited to less than one hour for adsorption prior to measurement.

There is evidence of desorption of the 6,000 MW PEO from the tip with successive measurements. Expulsion of PEO from the tip with each contact is expected. This creates bare spots on the surfaces reducing steric repulsion and allowing jump-in on approach to happen⁵⁰ from increasingly greater separation distances, Figure 26. The corresponding retraction traces on Figure 73 show bridging induced adhesion.

The 10,000 PEO sample's lack of such bridging adhesion and jump in/out (page 67) is evidence of contamination of tip #2, which would prevent PEO adsorption and explain the absence of measurable steric repulsion.

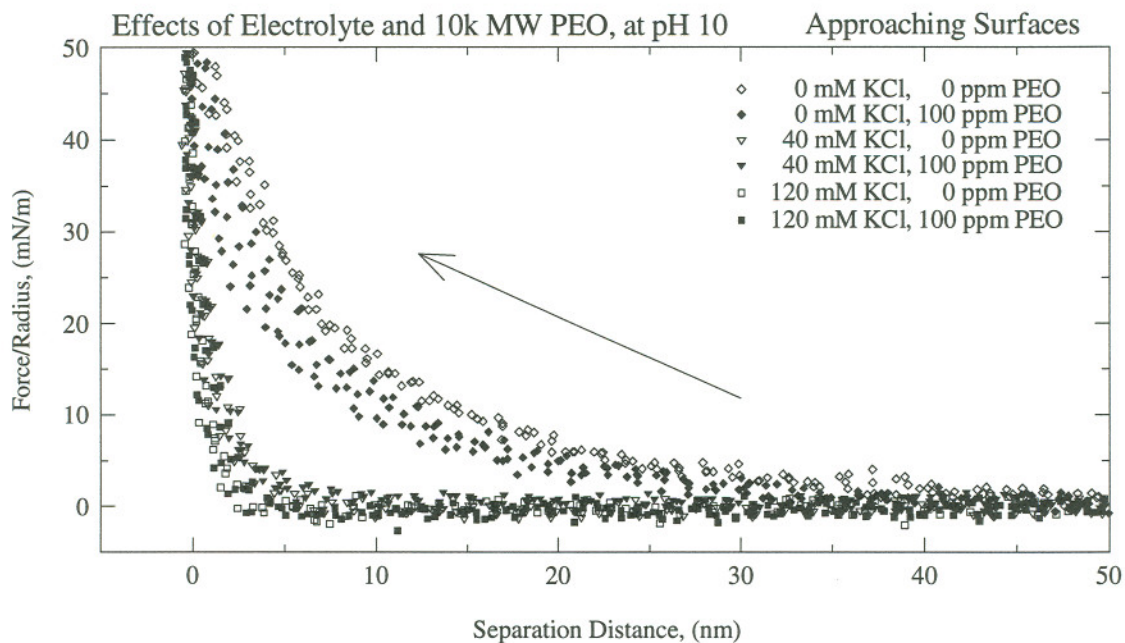


Figure 23. Electrostatic repulsive force decreases with increasing electrolyte concentration (hollow figures), as expected. 10k MW PEO does not appear to increase repulsion for approaching surfaces (solid figures).

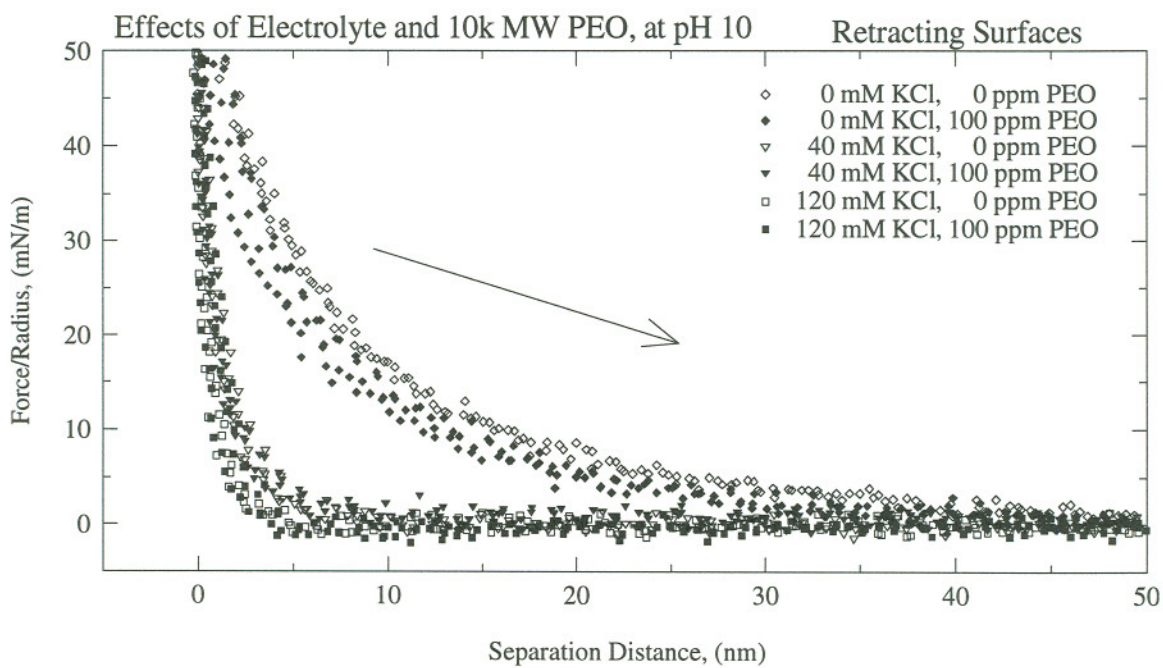


Figure 24. Retraction traces are very similar to approaching traces (previous figure) which suggests that 10,000 PEO has not adsorbed to surfaces. Adhesion on retraction is expected, as is displayed in the 6,000 MW sample.

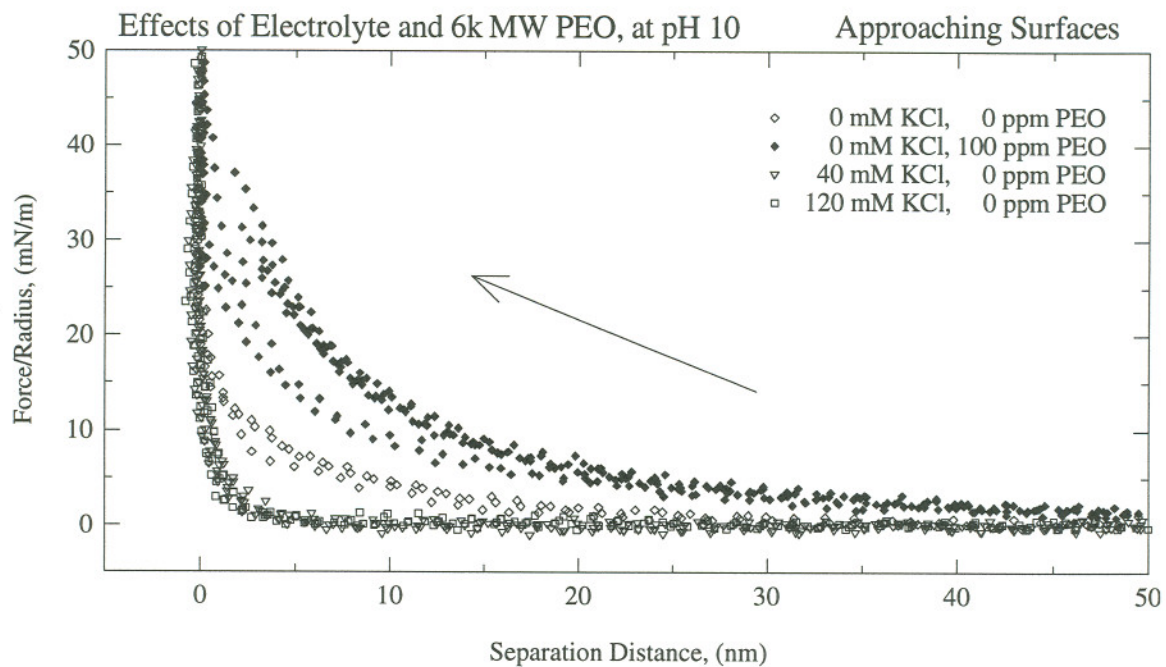


Figure 25. 6,000 MW PEO, approaching surfaces. HF etched wafer, Si_3N_4 tip #3. Addition of 6,000 MW PEO increases repulsion at low ionic strength. Within the PEO data set (solid diamonds) the first three traces recorded exhibit the greatest repulsion, the last three the least repulsion. Depletion of PEO from the tip with each contact (and insufficiently slow re-adsorption) probably accounts for the decreasing repulsion.

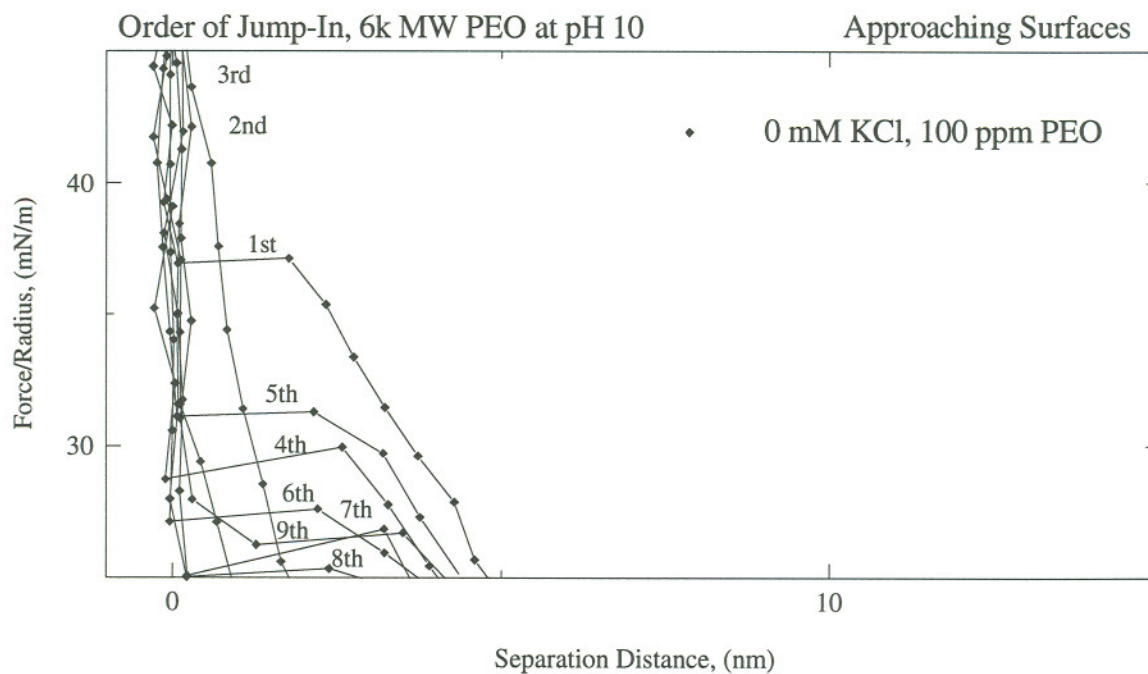


Figure 26. 6,000 MW PEO, approaching surfaces. HF etched wafer, Si_3N_4 tip #3. Addition of 6,000 MW PEO increases repulsion at low ionic strength. Detail of "jump-in" region of Figure 25 showing correlation between measurement number (1st - 9th) and propensity to jump-in. Depletion of PEO from the tip with each contact (and insufficiently slow re-adsorption) probably accounts for the decreasing repulsion. Progressive desorption or expulsion from the sample tip with each measurement facilitates short range attraction.

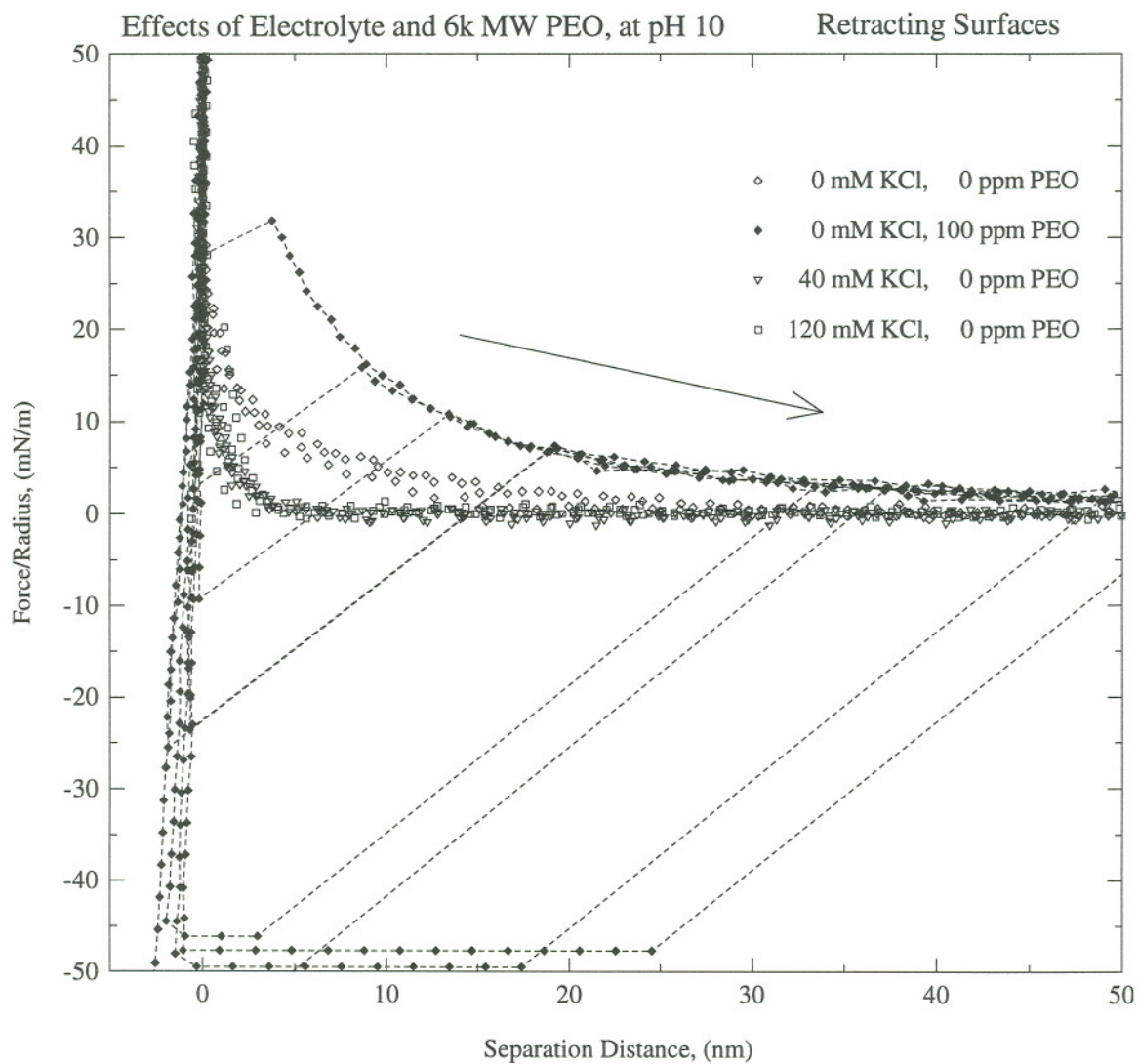


Figure 27. 6,000 MW PEO, retracting surfaces. HF etched wafer, Si_3N_4 tip #3. Strong adhesion is observed on retraction of the PEO samples (solid diamonds) indicating polymer bridging between the two surfaces. The order of measurement also correlates to increasing adhesion measurement: (left to right) 2nd, 1st, 3rd, 4th & 5th (superimposed), 6th, 9th, 8th, 7th.

CONCLUSION

As described in the last two paragraphs on page 12 (silanol condensation reaction), silica slurry particles can bond to wafers by either relatively weak physical or strong chemical mechanisms, where drying of the wafer shifts the preference from the former to the latter. This suggests that the wafers should not be allowed to dry until all reasonable attempts to remove wet slurry have been made, and that successful removal is much less likely once drying has occurred.

Deposition of wet slurry can be reduced by emersion through an IPA/water interface, as well as by hydrophobization of the wafer surfaces, inhibiting the entrainment of slurry particles.

Aside from chemical dissolution and ultrasonic water treatments (which may damage circuit layers), none of our attempts to remove dried untreated slurry were successful. When introduced in the rinse step, surface active agents can bind to the surface silanols and block the chemical silanol condensation reaction. Adsorbed agents can also augment the repulsion between wet wafer and slurry (e.g. PEO and steric repulsion) effectively improving the rinsing performance. We have demonstrated that the adsorption of such agents results in the reduction of dried adhesion strengths. This suggests that chemical bonding probably does occur in the untreated cases, and encourages such proactive approaches to adhesion prevention.

REFERENCES

1. Israelachvili, J., "Intermolecular & Surface Forces," 2nd ed. Academic Press, London, 1992
2. Adamson, A.W., "Physical Chemistry of Surfaces," 5th ed., John Wiley & Sons, Inc., New York, 1990
3. Meyers, D., "Surfaces, Interfaces, and Colloids: Principles and Applications", VCH, New York, 1991
4. Iler, R.K., "The Chemistry of Silica", John Wiley & Sons, Inc., New York, 1979
5. Israelachvili, J.N., *Chemica Scripta* **25**(1), 7 (1984)
6. Derjaguin, B.V., and Landau, L. *Acta Physiochim. URSS* **14**, 633 (1941)
7. Verwey, E.J.W., and Overbeek, J. Th. G., *Theory of Stability of Lyophobic Colloids*, Elsevier, Amsterdam, 1948
8. Guldbrand, L., Jonsson, B., Wennerstrom, H., and Linse, P., *J. Chem. Phys.* **80**(5), 2221 (1984)
9. From page 177 of reference 1, noting that $F(R) = -dW(R)$
10. Cook, L.M., *J. Non-Crystalline Solids* **120**, 152 (1990)
11. Riley, D.J., "Mechanisms of Particle Deposition From Ultrapure Liquids Onto Silicon Wafers", Ph.D. Thesis, North Carolina State University, 1992, UMI Dissertation Services, Ann Arbor MI
12. Sagiv, Jacob, *J. Amer. Chem. Soc.* **102**(1), 92 (1980)
13. Tripp, C.P., and Hair, M.L., *J. Phys. Chem.* **97**, 5693 (1993)
14. Tripp, C.P., and Hair, M.L., *Langmuir* **8**, 1961 (1992)
15. Tripp, C.P., and Hair, M.L., *Langmuir* **8**, 1120 (1992)
16. McGuir, J., Department of Bioresource Engineering, Oregon State University, private communication.

17. Churaev, N.V., and Derjaguin, B.V., *J. Colloid and Interface Sci.*, **103**(2), 542 (1985)
18. Frolov, Y.G., and Shabanova, N.A., *Langmuir* **3**, 640 (1987)
19. Fluck, D., Chemist, Cabot Corp., private communication regarding unpublished measurements.
20. Kosmulski, M. & Matijevic, E., *Langmuir* **8**, 1060 (1992)
21. Sugrue, S. *American Laboratory* **24**(6), 64 (1992)
22. Thompson, R.G., *American Laboratory* **24**(12), 48 (1992)
23. Neimczewski, B. *Ultrasonics* **18**(3), 107 (1980)
24. Heimenz, P.C., "Principles of Colloid and Surface Chemistry, 2nd ed.", Marcell Dekker, Inc., New York, 1986
25. Leenaars, A.F.M., "A New Approach to the Removal of Sub-micron Particles from Solid Substrates" in "Particles On Surfaces", V.1, pp.361-372, K.L. Mittal, Ed. Plenum Press, New York, 1986
26. McConnell, C.F., *Microcontamination* **9**(2), 35 (1991)
27. Israelachvili, J.N. & Pashley, R.M. *J. Colloid and Interface Sci.*, **98**(2), 500 (1984), and citations therein.
28. O'Connor, D.J., & Sanders, J.V., *J. of Colloid Sci.*, **11**, 158 (1956)
29. Tadros, Th.F., *J. Colloid and Interface Sci.*, **64**(1), 36 (1978), and citations therein.
30. Tadros, Th.F., *J. Colloid and Interface Sci.*, **46**(3), 528 (1974)
31. Lindquist, G.M., & Stratton, R.A., *J. Colloid and Interface Sci.*, **55**(1), 45 (1976)
32. Balayan, G.G., Avetisyan, M.S., and Tumanyan, N.P., *Zhurnal Prikladnoi Khimii (English translation)* **63**(7), 1538 (1990)
33. Hostetler, R.E., & Swanson, J.W., *Journal of Polymer Science* **12**, 29 (1974)
34. Dixon, J.K., La Mer, V.K., Li, C., Messinger, M., and Linford, H.B., *J. Colloid and Interface Sci.* **23**, 465 (1967)
35. Rubio, J. and Kitchner, J.A., *J. Colloid and Interface Sci.*, **57**(1), 132 (1976)
36. Milner S.T., *Science*, **251**, 905 (1991)

37. Claesson, P.M., Kjellander, R., Stenius, P., and Christenson, H.K., *J. Chem. Soc. Faraday Trans. 1*, **82**, 2735 (1986)
38. Björling, M, *Macromolecules* **25**, 3956 (1992)
39. Russel, W.B., in "Colloid-Polymer Interactions, Particulate, Amphiphilic, and Biological Surfaces, ACS Symposium Series, Vol. 532" Pp. 1-5 (P. Dubin & P. Tong, Eds.), American Chemical Society, Washington D.C., 1993
40. Stuart, M.A.C, Wajen, W.H.W., Cosgrove, T., Vincent, B., and Crowley, T.L., *Macromolecules*, **17**, 1825 (1984)
41. Killmann, E., Gutling, N., and Wild, TH. in "Polymer Adsorption and Dispersion Stability, ACS Symposium Series, Vol. 240", Pp. 357-376, (E.D. Goddard & B. Vincent, Eds.), American Chemical Society, Washington D.C., 1984
42. Hergeth, W.D., Zimmermann, R., Blos, P., Schmutzler, K., and Wartewig, S., *Colloids and Surfaces*, **56** 177 (1991)
43. Ducker, W.A. & Senden, T.J., *Langmuir* **8**, 1831 (1992)
44. Bergström, L. & Pugh, R.J., *J. Am. Ceram. Soc.* **72**(1), 103 (1989)
45. Horn, R.G., Smith, D.T., Haller, W., *Chemical Physics Letters*, **162**(4,5), 404 (1989)
46. Lin, Xue-Yun, Creuzet, F., Arribart, H., *J. Phys. Chem.* **97**, 7272 (1993)
47. Lea, A.S., Andrade, J.D., Hlady, V., in "Colloid-Polymer Interactions, Particulate, Amphiphilic, and Biological Surfaces, ACS Symposium Series, Vol. 532" (P. Dubin & P. Tong, Eds.), Pp. 266-279, American Chemical Society, Washington D.C., 1993
48. Klein, J., and Luckham, P.F., *Macromolecules* **17**, 1041 (1984)
49. Klein, J., and Luckham, P.F., *Nature* **308**, 836 (1984)
50. Lea, A.S., "Steric Exclusion Forces and Protein Imaging Using The Atomic Force Microscope", Ph.D. Dissertation, University of Utah, 1993